19

Dielectric and Transport Properties of Thin Films Deposited from Sols with Silicon Nanoparticles

Nickolay N. Kononov[1] and Sergey G. Dorofeev[2]
[1]*Prokhorov General Physics Institute, Russian Academy of Sciences, Moscow,*
[2]*Faculty of Chemistry, Moscow State University, Moscow,*
Russia

1. Introduction

Currently, there is steady scientific interest in structures formed by nanocrystalline silicon particles (*nc*-Si). This interest is to a large extent caused by the fact that efficient methods for fabricating silicon nanoparticles capable of bright and stable photoluminescence in the visible region of the spectrum with high quantum yield were developed over the last decade (Jurbergs at al., 2006). The main carriers of such nanoparticles are colloidal solutions (sols) based on methanol, chloroform, hexane, etc. Such sols are very promising objects for developing technologies for applying highly uniform thin *nc*-Si films onto various substrates. The use of such films seems very promising for developing light emitting elements based on *nc*-Si electroluminescence (Anopchenko at al., 2009). Furthermore, *nc*-Si films are very promising as elements of solar panels (De la Torre at al., 2006), thin film transistors (Min at al., 2002), and single electronic devices (Tsu, 2000). In the case in which films consist of nanoparticles with a diameter smaller than 10 nm, their total characteristics are controlled not only by their material, but also by properties of atoms on the surface of these particles. In other words, in general, such films should be considered as a multicomponent medium the properties of which are controlled by both crystalline cores of nanoparticles and surface atoms and molecules and air voids being a film component.

In the modern scientific literature, most papers are devoted to the study of properties of amorphous silicon (a-Si) films with introduced silicon nanocrystals (Conte at al., 2006; Wang at al., 2003). Such films can be deposited, e.g., in the high frequency discharge in a mixture of gases SiH4, Ar, or H2 (PECVD method), followed by high temperature annealing (Saadane at al., 2003).

Recently, we showed that homogeneous thin films (with a thickness up to 30 nm) can be grown by size selective precipitation sols containing nanocrystalline silicon particles (Dorofeev at al., 2009). Such films (*nc*-Si) are formed by closely adjacent crystalline Si nanoparticles; therefore, their physical characteristics to a certain extent should be similar to characteristics of films based on porous silicon (por-Si). The optical absorption and photoluminescence ability of por-Si films have been very comprehensively studied to date (see, e.g., Kovalev at al., 1996; Brus at al., 1995); however, the number of studies of transport

and dielectric properties of such films in an ac electric field is extremely small. Here we indicate papers (Axelrod at al., 2002; Ben-Chorin at al., 1995; Urbach at al., 2007) devoted to such studies of por-Si.

A similar situation exists as applied to *nc*-Si films; however, we are not aware of results of studies on the conductivity in an ac electric field (ac conductivity and dielectric relaxation in such films).

In this chapter we analyze the dielectric and transport properties of nc-Si films deposited on a glass and quartz substrates from the sol containing nanoparticles of silicon. Silicon nanoparticles were synthesized in the process of laser pyrolysis of silane and placed in ethanol or methanol, repeatedly centrifuged resulting in a colloidal solution (sol) in which the silicon nanoparticles could be a long time (over two years). We analyze three kinds of films. The films deposited on a substrate by centrifugation of sols of nanoparticles in a week after their synthesis. Films deposited on a substrate of sols in which the nanoparticles were 2 years after their synthesis and films deposited from two-year-old sol in which has been added the conductive tetra-aniline. More circumstantial experimental details we will present in the following sections. In the future of the films deposited on a substrate of silicon nanoparticles in a week after their synthesis we call films I, films obtained from similar nanoparticles, but two years after their synthesis (aged nanoparticles) - films II and films deposited of sols with aged nanoparticles and with the tetra aniline addition - films III.

For films I we present measurements of the *nc*-Si film permittivity in the optical range ($5\times10^{14} \le \nu \le 10^{15}$ Hz) and in the frequency range of $10 \le \nu \le 10^{6}$Hz. In the latter range, the ac conductivity (σ_{ac}) of *nc*-Si films is also determined.

In the optical region, the real ε' and imaginary ε'' components of the complex permittivity were determined from an ellipsometric analysis of light beams incident and reflected from the free boundary of the *nc*-Si film. In the frequency range of $10 \le \nu \le 10^{6}$ Hz, the ε' and ε'' spectra, were determined from an analysis of the frequency dependence of the *nc*-Si film impedance.

In an optical spectral region, ε' and ε'' varied within 2.1–1.1 and 0.25–0.75, respectively, as the frequency increased. We attribute such low values of ε' and ε'' to the *nc*-Si film structure. The *nc*-Si particles forming such films consist of crystalline cores surrounded by a SiO_x shell ($0 \le x \le 2$). The SiO_x shell results from the interaction of the Si nanoparticle surface with ambient air. On the basis of the analysis of the Raman spectra, it is suggested that the amorphous component is involved in the *nc*-Si powders and films due to oxygen atoms arranged at the nanoparticle surface.

Using the Bruggeman effective medium approximation (EMA) (Bruggeman, 1935), the structural composition of *nc*-Si film was simulated. It was shown that good agreement between the frequency dependences of ε' and ε'' obtained from the EMA and the ε' and ε'' spectra determined from ellipsometric data is achieved when *nc*-Si films are considered as a two component medium consisting of SiO and air voids existing in it. In the frequency range of 10–10^{6} Hz, the ε' and ε'' dispersion was determined from an analysis of the frequency dependences of the capacitance of *nc*-Si films and their impedance spectra. It was found that ε' and ε'' vary within 6.2–3.4 and 1.8–0.08, respectively, as the frequency increases.

It is found that the function ε'(ω) in this frequency range is well approximated by the semiempirical Cole–Cole dependence (Cole–Cole dielectric relaxation) (Cole, K. S. & Cole, R. H., 1941). At the same time, the ε''(ω) spectra of *nc*-Si films are well approximated by the Cole–Cole dependence only at frequencies higher than 2×10^2 Hz. In the low frequency spectral region, good approximation is achieved by combining the Cole–Cole dependence and the term associated with the presence of free electric charges. From analysis of the approximating dependences, the average room temperature relaxation times of dipole moments in *nc*-Si films were determined as 6×10^{-2} s.

The conductivity σ_{ac} of the studied films I in an ac electric field depends only on its frequency according to the power law; the exponent is 0.74 in the entire frequency range under study. Such behavior of σ_{ac} suggests that the electrical transport mechanism in films is hopping. Comparison of the measured frequency dependence $\sigma_{ac}(\nu)$ with similar dependences following from various models of hopping conductivity shows that the $\sigma_{ac}(\nu)$ behavior is most accurately described in the diffusion cluster approximation (DCA) (Dyre & Schrøder, 2000; Schrøder & Dyre, 2002; Schrøder & Dyre, 2008).

Analysis of the dependences of the dark conductivity of films on humidity of ambient air and the temperature dependence of absorption bands caused by associated Si–OH groups on the film surface allowed the conclusion to be drawn that conductivity at frequencies lower than 2×10^2 Hz is associated with proton transport through the hydrogen bound hydroxyl groups on the silicon nanoparticle surface.

For films II and III we present measurements of the *nc*-Si film permittivity and ac conductivity (σ_{ac}) in the frequency range of $1 \leq \nu \leq 10^6$Hz. The dielectric properties of the films II and III were studied by impedance spectroscopy only in the frequency range $1 \leq \nu \leq 10^6$Hz.

We found that in films II and III, a double dielectric relaxation exists and to adequately describe the spectra of ε 'and ε'' of these films should use not only the Cole-Cole relationship, but and the law of Debye's dielectric relaxation.

By a total approximation of the experimental spectra of the films II and III the values of static dielectric constant ε_0 have obtained. These values are equal 11.5 and 67 respectively. Value $\varepsilon_0 \approx 11{,}5$ characteristic of film II is close to the static permittivity of crystalline silicon, but the magnitude of $\varepsilon_0 \approx 67$ of films III significantly higher than this value. Next, we analyze this fact.

In contrast to the conductivity of the films I σ_{AS} of films II and III are not subject to a power law over the entire range of measured frequencies. Next, we show that such a deviation from the law $\sigma_{AS} \sim \omega^s$ associated with the appearance in the spectra ε "(ω) of the films II and III Debye's components.

2. The films from silicon nanoparticles

2.1 Films deposited from freshly prepared sols of silicon nanoparticles (films I)

2.1.1 Samples and measurement procedures

The *nc*-Si films were deposited from silicon nanoparticles produced by CO_2 laser pyrolysis of silane. The system for synthesis of the *nc*-Si powders and conditions of the process are described in detail elsewhere (Kononov at al., *2005*; Kuz'min at al., 2000). In what follows,

we briefly outline the procedure of synthesis of the Si nanoparticles. In a reactor chamber filled with a buffer gas (helium or argon) to the pressure P = 200 Torr, a fine SiH_4 jet is formed and heated by focused cw CO_2 laser radiation beam crossing the jet. During pyrolysis of silane, the SiH_4 molecules are decomposed, and free Si atoms are produced. When colliding with each other and with the atoms of the buffer gas, the Si atoms form particles, whose average dimensions can be in the range from 10 to 100 nm, depending on the pressure of the buffer gas. The *nc*-Si powders produced in such a manner were dispersed by ultrasonic treatment in ethanol and centrifuged for 30 min with an acceleration of 2000g (g is the gravitational acceleration). As a result, almost all agglomerates of *nc*-Si particles are precipitated. After preliminary centrifugation, a stable colloidal solution (sol) of *nc*-Si in ethanol remains. No visible changes in the solution, including precipitations, were observed for two years. For the subsequent deposition of nanoparticles, a water solution of aluminum dihydrophosphate was added to the sol.

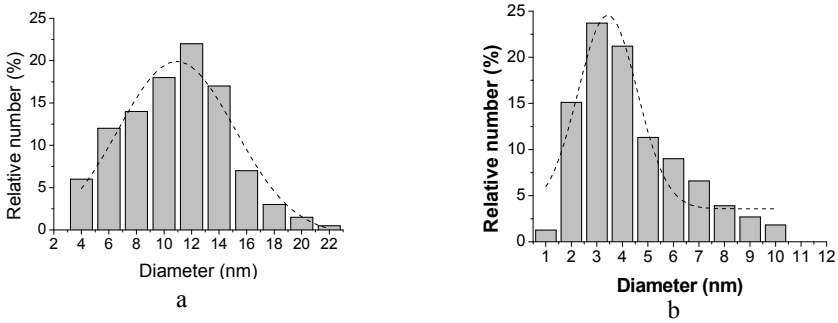

Fig. 1. (a) Histogram of the size distribution of particles, as obtained by processing of the TEM images of the *nc*-Si powder (b) Histogram of the size distribution of particles, as obtained by processing of the TEM images of the *nc*-Si powder etched in the (HF + HNO_3) acid mixture. The dushed lines represent the normal distribution functions for two different kinds of nc-Si particles

The size distribution of *nc*-Si particles was determined from images obtained using an LEO 912 AV OMEGA transmission electron microscope. The typical spectrum of silicon nanoparticles used for precipitation is shown in the Fig. 1. The *nc*-Si film thickness was determined using a Taly Step (Taylor-Hobbson) atomic force step profilometer. Ellipsometric spectra were measured using an Ellips 1891 ellipsometer (Institute of Semiconductor Physics, Siberian Branch, Russian Academy of Sciences). The transmission spectra were measured using a Lambda 900 (Perkin-Elmer) spectrophotometer. The Raman spectra of the films were recorded with a microlens equipped T 64000 (Jobin Ivon) Raman triple spectrograph in the backscattering layout of measurements at the power of the excitation argon laser 2 mW.

The impedance spectra were measured using an E7-20 immittance meter (Minsk Research Instrument Making Institute) and a Z-3000X (Elins) impedance meter. Samples for

measuring impedance spectra were prepared as follows. First, aluminum electrodes separated by a rectilinear gap 1 mm wide were deposited on a glass substrate. Then *nc*-Si particles were precipitated from the sol on the substrate prepared in such a way, which formed a film. The third aluminum electrode was deposited on the obtained *nc*-Si film. As a result, a sandwich like structure similar to that shown in Fig. 2 was obtained. To achieve the ohmic lead contacts, the structure was annealed at a temperature of 400°C and a pressure of 10^{-5} Torr. Impedance spectra were measured at an amplitude voltage of 100 mV; however, the films under study can withstand a voltage to 15 V without electrical breakdown.

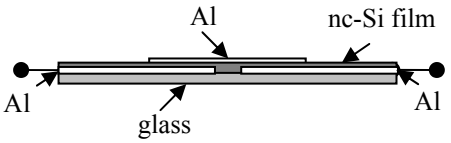

Fig. 2. Diagram of the sandwich like sample structures for measuring impedance spectra.

2.1.2 Experimental results

2.1.2.1 Raman scattering

To record the Raman spectra, we first deposited an aluminum film with the thickness ~300 μm onto the quartz substrate, and then, on top of the film, we deposited the *nc*-Si film from the sol. We proceeded in such manner in order to avoid the background scattering component produced by the quartz substrate. In this section, we analyze the Raman

spectra recorded for the initial *nc*-Si powder, for the films deposited at the second stage of centrifuging the sols of the initial *nc*-Si powder and film deposited from the sol with powder etched in the (5wt%**H**F+14wt%HNO_3) water mixture. The corresponding samples are identified as samples S_1, S_2, and S_3 respectively.

The typical Raman spectra recorded for these samples are shown in Fig. 3. All of the experimentally recorded spectra are very similar to the Raman spectra obtained for *p*-Si in (Tsang at al., 1992; Tsu at al., 1992) and for the *nc*-Si clusters in (Ehbrecht at al., 1995).

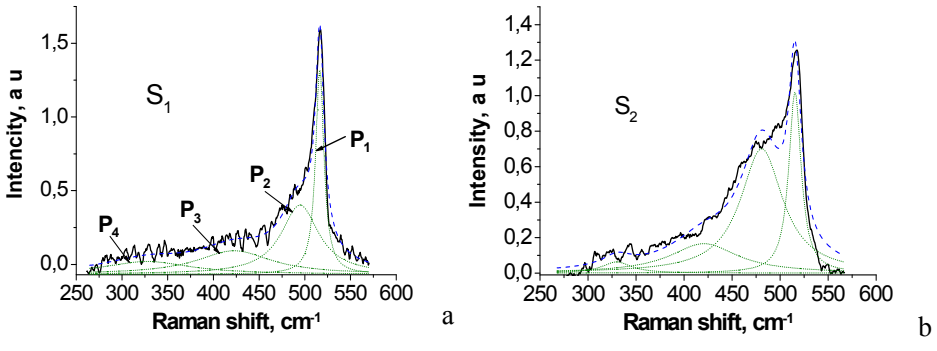

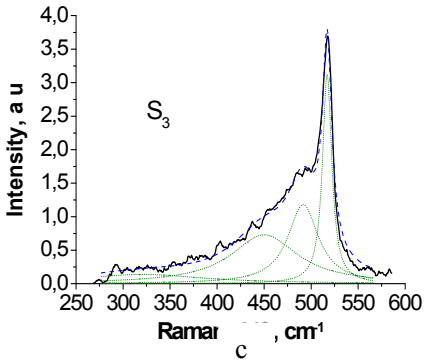

Fig. 3. Raman spectra of: a) nc-Si powder S_1, b) film deposited from the sol of the initial *nc*-Si powder-S_2 c) film deposited from the sol *nc*-Si powder etched in the (HF + HNO_3) acid mixture –S_3. The dotted line refers to the approximation of the spectrum with Lorentzian contours (the *P*1, *P*2, *P*3, and *P*4 peaks).

The Raman spectra of all of the samples studied here can be fitted with four Lorentzian bands with a rather good accuracy (Fig. 3). In what follows, these bands are referred to as the P_1, P_2, P_3, and P_4 peaks. The Raman shift of the most intense P_1 peak with respect to the emission frequency of the probing laser is in the range of wave numbers from 515 to 517 cm^{-1} for all of the samples. The Raman shift of the similar peak for *c*-Si corresponds to the wave number 520.5 cm^{-1}. Thus, for all of the films studied here, the P_1 peak is shifted to smaller wave numbers with respect to the peak for *c*-Si (the red shift). The P_1 peak in the Raman spectra of the *nc*-Si particles is due to light scattering assisted by longitudinal optical (LO) and transverse optical (TO) phonons at the central point of the Brillouin zone for the *c*-Si crystal lattice. The red shift of the P_1 peak and its half width as functions of the nanoparticle dimensions are adequately described in the context of the phonon's confinement model (Campbell & Faushet 1986; Richter at al., 1981).

The result of application of this model to spherical nanoparticles is shown in Fig. 4. From Fig. 4, it can be seen that the average dimension of the *nc*-Si particles in the samples is in the range 4–6 nm, irrespective of whether the particles of the initial *nc*-Si powder were subjected to some treatment or not. For the sols of the *nc*-Si powders etched in the (HF + HNO_3) mixture, the average particle's dimensions determined in the phonon's confinement model are in good agreement with the particle dimensions corresponding to the peak of size distribution obtained for the particles by processing of the TEM images.

However, for the initial *nc*-Si powders, the average particle dimensions determined by the above mentioned two methods differ by a factor of about 2. There are two possible causes of the difference between the average particle's dimensions determined in the phonon's confinement model and by processing of the TEM images. One of the causes is associated with the fact that, in the phonon's confinement model, the nanoparticles are assumed to be single crystals. Therefore, the magnitude of the phonon wave's vector q in the

nanoparticle can vary in the range $(0, 2\pi/L)$, where L is the particle diameter. However, if the nanoparticle core is polycrystalline and the average dimension of the elementary crystal lattice in the core is l, the confining condition $q \leq 2\pi/L$ should be replaced by the condition $q \leq 2\pi/l$. Thus, it is possible that the dimensions l = 4–6 nm calculated in the phonon's confinement model are related to the average dimensions of elementary lattices in the polycrystalline nanoparticle cores rather than to the average nanoparticles' dimensions in the initial *nc*-Si powder. From this assumption and the fact that, for nanoparticles subjected to etching, the average dimensions determined by the above two methods are the same, it follows that, on such etching of the nanoparticles, the remaining *c*-Si cores are single crystals. The other cause can follow from the well known low contrast of the finest nanoparticles (with the diameter 3 nm in the case under study) in the TEM images. Because of the low contrast, the processing of the TEM images always reduces the relative portion of the fine grained fraction of nanoparticles in the ensemble of particles under consideration.

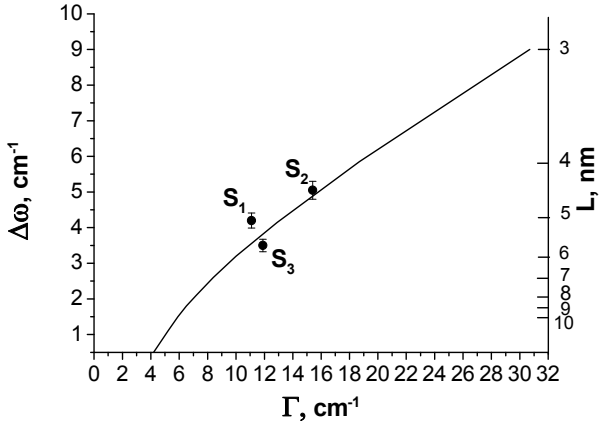

Fig. 4. The half-width and the red shift of the P_1 Raman peak versus the diameter of the spherical silicon nanoparticles, as obtained (solid line) in the context of the phonon's confinement model [19, 20] and (solid circles) from the approximation of the P_1 peak in samples S_1, S_2 and S_3, with the Lorentzian contours.

The Raman shift of the P_2 peak in the samples is in the range from 480 to 495 cm^{-1}. This peak corresponds to the TO-phonon assisted scattering in *a*-Si:H. Similarly to the P_2 peak, the P_3 and P_4 peaks are related to the amorphous component of the structure of the Si particles and result from scattering assisted by LO and longitudinal acoustic (LA) phonons.

From the comparison of the integrated intensities of the P_1 and P_2 peaks, *Ic* and *Ia*, we can determine the volume fraction of the crystalline phase, *Xc*, in the Si particles. To do this, we used the expression (Voutsas at al., 1995)

$$\mathbf{X_c} = \frac{\mathbf{I_c}}{\mathbf{I_c} + \eta \mathbf{I_a}} \tag{1}$$

where $\eta = \frac{\sigma_{\mathbf{c}}}{\sigma_{\mathbf{a}}}$ is the ratio between the integrated backscattering's cross sections in the crystalline and amorphous fractions (corresponding to the P_1 and P_2 peaks). According to (Kakinuma at al., 1991), the quantity η for silicon is η = 0.8–0.9. In the calculations, we set η = 0.8. For samples S_1, S_2 and S_3, the values of the parameter Xc are 0.45, 0.35 and 0.50 respectively.

From these values of X_c, it follows that almost a half of the volume of the particles is characterized by a high degree of disorder of the crystal lattice.

From comparison of the above values, it is evident that, in film S_2 deposited at the second stage of centrifuging from the sol with the initial *nc*-Si powder, the parameter X_c is smaller than X_c for the initial powder. The average particle's dimension in film S_2 is smaller than that in the initial powder. Correspondingly, the surface area to volume ratio for the particles in the S_2 film is larger than the corresponding ratio in the initial powder. Therefore, the effect of the nanoparticle surface on the general properties of the nanoparticles in film S_2 is bound to be more pronounced that the corresponding effect in the initial powder. Consequently, the smaller value of X_c (the higher degree of amorphization of the particles) in film S_2 in comparison with X_c in sample S_1 suggests that the disordered regionis at the nanoparticle surface rather than in the nanoparticle core. However, for film S_3 the value of X_c is larger than X_c for film S_2, although the average particle's dimensions in these films are comparable. Such difference suggests that the degree of disorder of particle surfaces in film S_3 is lower than that in film S_2.

Since film S_3 are deposited from the sols of the *nc*-Si powders subjected to etching, such lower degree of disorder in these films is due to the effect of the HF and HNO_3 acids on the particle surface. Here, it is reasonable to mention the studies (Luppi & Ossicini, 2005; Puzder at al., 2002), in which the effect of oxygen atoms on the structure of silicon clusters and on the degree of ordering of the Si crystal lattice in nanoparticles is analyzed, and the studies (Ma at al., 2000 Tsang at al., 1992;), in which the changes induced in the Raman peak similar to the P_2 peak (Fig. 3) by the effect of oxygen on the surface of *p*-Si passivated with hydrogen, are reported. The general idea of the above mentioned studies is that the crystal lattice of nanoparticles, whose surface is completely passivated with hydrogen, is practically the same as the lattice of the silicon crystal. However, if oxygen atoms appear at the nanoparticle surface, they can form the Si–O–Si and (Si=O) bonds and, thus, distort the lattice at the distances up to 0.5 nm. In this space region, the distortions of angles between the Si–Si bonds in the crystal lattice can be as large as 10° (Tsang at al., 1992). Therefore, if the surface of a nanoparticle of a diameter smaller than 3 nm is coated with the SiO_2 oxide, the crystal lattice is distorted within a noticeable volume fraction of such particle. As a consequence, if the *p*-Si surface is etched in the solution of HF, the Raman spectrum involves only one peak similar to the P_1 peak. If *p*-Si is exposed to oxygen in oxygen containing atmosphere, the Raman spectrum exhibits also the P_2 peak along with the P_1 peak. From the above mentioned studies and from the analysis of the Raman spectra discussed here, we can make the statement presented below. At the surface of *nc*-Si nanoparticles in all samples, there is a noticeable number of oxygen atoms, which distort the crystal lattice in these particles and bring about the appearance of the P_2 peak in the Raman spectra. Since the average nanoparticle's dimensions in film S_2 are smaller than those in powder S_1, the effect of these oxygen atoms on the crystal lattice structure in film S_2 is more pronounced than the

effect in powder S_1. As a result, the volume fraction of the crystal phase in film S_2 is reduced compared to that in S_1.

Etching of the *nc*-Si particles in the solution of the (HF + HNO_3) acids results in a decrease in the particle dimensions. However, in this case, the total number of oxygen atoms at the nanoparticle's surface decreases, since a portion of oxygen atoms is replaced with hydrogen atoms. Therefore, in film S_3 two opposite processes are bound to occur. One process related to the decrease in the nanoparticle's dimensions yields a decrease in *Xc*, whereas the other process related to the decrease in the number of oxygen atoms at the nanoparticle surface brings about an increase in *Xc*. In film S_3, we experimentally observe the parameter X_c larger than X_c in film S_2; therefore, we can conclude that, on etching of the *nc*-Si particles, the latter process dominates over the former one.

2.1.2.2 Ellipsometric spectra

In the experiment, the ellipsometric angles ψ and Δ were measured as functions of the wavelength of a light beam incident at the angle Φ_0 on the free flat surface of the *nc*-Si film. The films under study were applied on glass and quartz substrates and on quartz substrates with preliminarily deposited aluminum films. The *nc*-Si film thicknesses (1–2 μm) were measured independently. When processing the ellipsometric data, the *nc*-Si films under study were considered as a 3D medium in air medium. The complex refractive index $N = n - ik$, where n is the film refractive index and k is the extinction coefficient, was determined by the expression (Azzam & Bashara, 1977)

$$N = N_0 \sin \Phi_0 \sqrt{1 + \left(\frac{1-\rho}{1+\rho}\right)^2 tg^2 \Phi_0} \tag{2}$$

Here, $\rho = e^{i\Delta} \cdot tg\psi$ and N_0 are the complex refractive index of an ambient medium (air), which was equal to unity in the case at hand. It is known that formula (2) yields accurate values only when light is reflected from a semi-infinite medium with a boundary with an atomically clean surface. If impurities or an oxide filmare on the boundary, they introduce errors to the calculated values. In (Tompkins & Irene, 2005), the values n and k were compared for crystalline silicon (*c*-Si) in the absence and presence of the oxide film on its surface. It follows from this comparison that, in the presence of a SiO_2 film to 2 nm thick on the silicon surface, the value of n is almost identical to that of *c*-Si in the incident photon energy range of 1–3.4 eV; in the range of 3.4–5 eV, the refractive index differs from n of *c*-Si no more than by 20%, as well as k. However, in the range of 1–3.4 eV, the value of k in the presence of the SiO_2 film almost twice exceeds the *c*-Si extinction.

Since the real ε' and imaginary ε'' components of the medium permittivity are related to n and k by the known expressions $\varepsilon' = n_2 - k_2$ and $\varepsilon'' = 2nk$, it can be expected that the values of ε' calculated by Eq. (2) for *nc*-Si films will be slightly systematically underestimated, while the values of ε'' will be overestimated.

Nevertheless, representation of the pseudo dielectric functions by relation (2) is very convenient and is quite often used to study the dielectric properties of materials. For example, dielectric parameters of *por*-Si were studied using this equation in (Pickering, 1984). As applied to the present study, an analysis of the spectra obtained using formula (2)

was limited by the energy range of incident photons, in which films strongly absorbed incident probe radiation, which could not reach the substrate surface in this case. If probe radiation reached the substrate surface with precipitated film, an interference structure arose in the spectra, which consisted of alternating minima and maxima. Such a structure at energies lower than 2 eV is easily seen in Fig. 5 (curves *3* and *3* ').

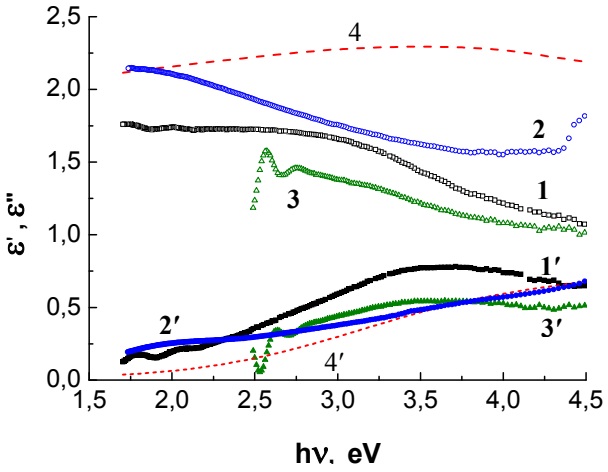

Fig. 5. Spectra of (*1*–*3*) real and imaginary (*1*'–*3*') permittivity components of *nc*-Si films precipitated on various substrates: (*1*, *1*') film of initial (unetched) nanoparticles on the glass substrate; (*2*, *2*') film of nanoparticles preliminarily etched in a HF/HNO_3 acid mixture on the quartz substrate; (*3*, *3*') *nc*-Si film of initial nanoparticles on the glass substrate with a preliminary deposited aluminum film; and (*4*, *4*') Bruggeman approximation for ε' and ε'', respectively.

We can see the spectra of pseudo dielectric functions ε' and ε'' of *nc*-Si films fabricated by precipitating initial silicon nanoparticles on the glass substrate and nanoparticles preliminary etched in a HF/HNO_3 acid mixture in a water for 30 min on the quartz substrate. Figure 5 also shows the ε' and ε'' spectra of *nc*-Si films precipitated on the glass substrate with a preliminarily deposited aluminum film.

It follows from this figure that the obtained values of ε' and ε'' are significantly lower than the similar values of *c*-Si.

Figure 6 shows the absorption spectra α(*E*) of the same films, obtained by the relation:

$$\alpha(E) = \frac{4\pi\nu}{c}k = \frac{4\pi E}{ch}k \tag{3}$$

where $E = h\nu$ is the energy of the incident photon and k is the experimentally measured extinction coefficient.

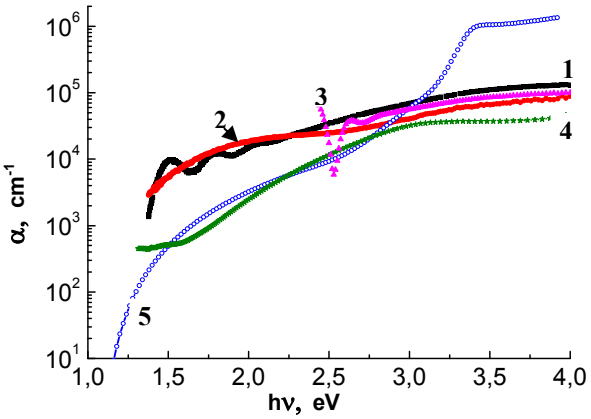

Fig. 6. (*1*–*3*) - absorption spectra of *nc*-Si films, obtained from ellipsometric data; (*4*) - absorption spectrum of film 1, obtained from its transmission spectrum; and (*5*) - absorption spectrum of crystalline silicon.

This figure also shows the absorption spectrum of the *nc*-Si film formed by unetched nanoparticles, which was calculated from its transmission spectrum. As a reference, the absorption spectrum of crystalline silicon (Aspens & Studna, 1983) is also shown. The size distribution of unetched and etched *nc*-Si particles used to precipitate films 1 and 3 are shown in Fig. 1.

A comparison of the absorption spectra of the film *nc*-Si grown from unetched nanoparticles, which were obtained from ellipsometric measurements and by processing the corresponding transmission spectrum, shows that the values of α obtained by ellipsometry are higher than the similar values calculated from transmission spectra, and this difference increases with decreasing the incident photon energies. As noted above, this difference is associated with the error of the extinction coefficient calculation by formula (2). At the same time, both spectra exhibit strong absorption of the *nc*-Si film in comparison with *c*-Si at energies lower than 1.5 eV. Such absorption enhancement in the low energy photon region is also inherent to the film grown by etched nanoparticles. At energies higher than 3 eV, all spectra exhibit absorption weaker than that of *c*-Si. In the Fig. 1, we can see that the diameter of an appreciable fraction of particles used to form films is smaller than 10 nm; therefore, the most probable cause of a decrease in the film absorption in the high-energy photon region is widening of the band gap in crystalline cores of silicon nanoparticles due to quantum confinement.

2.1.2.3 Dielectric dispersion

The permittivity spectra of *nc*-Si films were calculated from the measured frequency dependences of the capacitance of corresponding samples and their impedances, $Z(\nu) = Z' - iZ''$, $Z(\nu) = U(\nu) / I(\nu)$,

where $U(\nu)$ is the potential difference at sample electrodes and $I(\nu)$ is the current flowing through the sample.

In what follows, we will analyze the dielectric properties of the Al–*nc*-Si–Al sandwich system in which the *n*-Si layer was precipitated from the sol with unetched nanoparticles. The thickness of this film was 2 μm; the geometrical capacitance of this system was $C_0 = 1.15 \times 10^{-10}$ F. The dielectric dispersion of this film is typical of other films obtained in a similar way from similar *nc*-Si particles.

Figure 7 shows the frequency dependence of the capacitance of this system. The capacitance was measured in parallel connection. The figure also shows the spectrum of the real component $\varepsilon'(\nu)$ of the film permittivity, calculated from the relation $\varepsilon' = C(\nu)/C_0$.

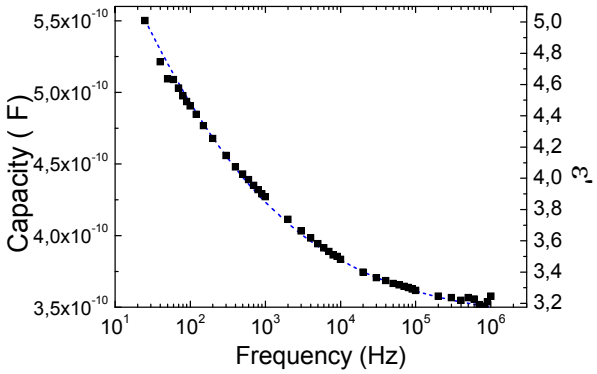

Fig. 7. Frequency dependence of the *nc*-Si film capacitance. The dashed curve is the approximation by function (3) (see text).

The $\varepsilon'(\nu)$ and $\varepsilon''(\nu)$ spectra of *nc*-Si films were also determined from the frequency dependence the film impedance by the expression

$$\varepsilon = \varepsilon' - i\varepsilon'' = \frac{1}{i2\pi\nu C_0 Z(\nu)} \tag{4}$$

Figure 8.a shows the dependences $\varepsilon'(\nu)$ and $\varepsilon''(\nu)$ calculated by the above method for the film under study. A comparison of the values of $\varepsilon'(\nu)$ obtained from $C(\nu)$ and $Z(\nu)$ measurements shows good quantitative and qualitative agreement of the values calculated in two different ways; in both cases, in the frequency range of $10 \le \nu \le 10^6$ Hz, the value of $\varepsilon'(\nu)$ is within 6–3.4 and decreases with frequency.

2.1.2.4 AC conductivity of films I

The ac conductivity of *nc*-Si films was determined by the known relation

$$\sigma_{AC}(\nu) - \sigma(0) = \varepsilon_0 \cdot \varepsilon''(\nu) \cdot 2\pi\nu$$

where $\sigma(0)$ is the dark conductivity of films in a dc electric field and $\varepsilon_0 = 8.85 \times 10^{-12}$ F/m is the permittivity of free space. The value of $\sigma(0)$ of the film under study at room temperature

(T = 297 K) was 9×10^{-10} Ω^{-1} m^{-1} and was used to calculate $\sigma_{AC}(\nu)$. The dependence $\sigma_{AC}(\nu)$ is shown in Fig. 9 on a log scale.

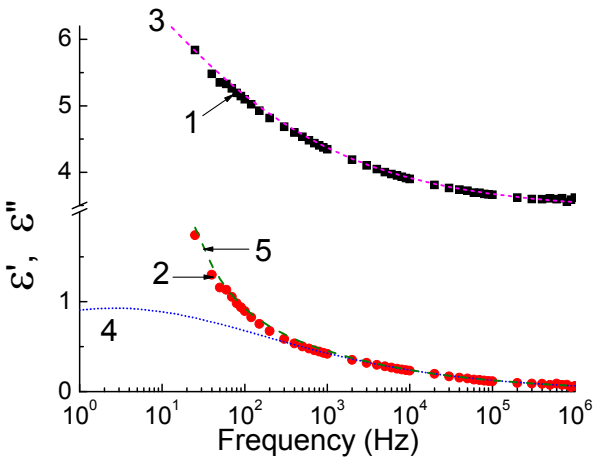

Fig. 8a. (*1, 2*) Frequency dependences of ε' and ε'', obtained from impedance spectra. Cole–Cole approximation of ε' - (*3*) and ε'' spectra (*4*) without and (*5*) with consideration of the contribution of free carriers.

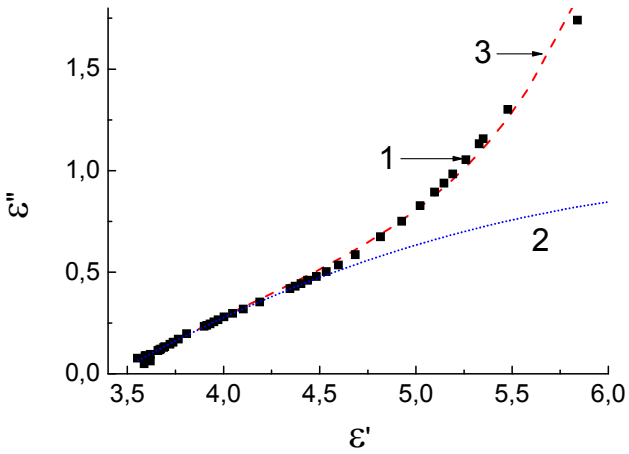

Fig. 8b. (*1*) Dependence ε''(ε') for the *nc*-Si film. Cole–Cole approximation (*2*) without and (*3*) with consideration of the contribution of free carriers.

This figure suggests that $\sigma_{AC}(\nu)$ can be well approximated by the power law dependence with an exponent of 0.74.

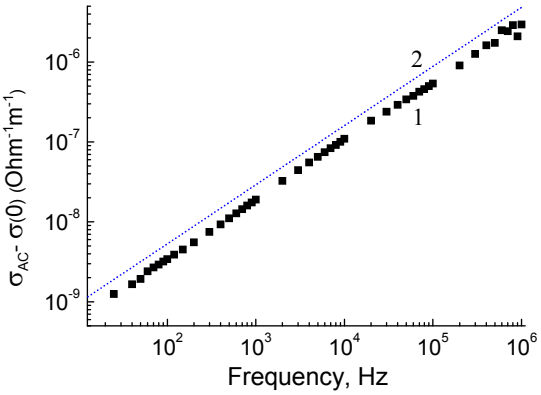

Fig. 9. (*1*) Frequency dependence of the ac conductivity of the *nc*-Si film; (*2*) dependence $\sigma_{ac}(v)$ defined by the DCA model (see text) using experimentally measured ε_s, ε_∞, and $\sigma(0)$.

2.2 Films deposited from aged nc-Si sols (Films II) and from aged nc-Si sols with tetraaniline (Films III)

2.2.1 Samples

The previous sections have presented experimental results of a study of thin films obtained from nanoparticles synthesized by one week prior to their deposition on the substrate. As already mentioned silicon nanoparticles could be no precipitation of sols for a long time. By the time of this writing, the silicon nanoparticles used for the deposition of films analyzed in the previous sections, were in sols over two years and in the next section we will report on the results of studies of the properties of the films deposited on substrates of these sols. It should be noted here that the film deposited on a substrate not as a result of centrifugation of sols, and with the spin coating method. Also in the following sections we will analyze the dielectric properties of films deposited from a 2-year nc-Si sols, in which the conductive tetramer – tetraaniline was added (Wang & MacDiarmid, 2002).

Because pure tetraaniline has low conductivity, for its increase the tetra aniline doped with p-toluensulfonic acid ($CH_3(C_6H_4)SO_3H$). Briefly the process of doping was as follows. A solution of tetraaniline and dimethyl sulfoxide (DMSO) as a solvent mixed with a DMSO solution of para-toluenesulfonic acid, so that the resulting solution in the molar ratio of tetra aniline and acid was 1.5. At the end of doping the color of resulting solution became green. The conductivity of the film which was deposited on a substrate of resulting tetraaniline solution was at room temperature 10^{-4} Ohm^{-1}m^{-1}. The resulting solution of tetraaniline in DMSO was added to the sol of silicon nanoparticles in ethanol in a mass ratio 1:10 before deposition of film on substrates.

As we have already reported, the films deposited on a substrate of silicon nanoparticles in a week after their synthesis we call the films I; films, obtained from the same nanoparticles, but two years after their synthesis (aged nanoparticles) - films II and films with aged nanoparticles and addition of tetraaniline - films III. Before the measurement the sandwich

like structures of the films II and III with Mg or Al electrodes were heated to a temperature of 140^0 C and held at that temperature for 30 minutes.

2.2.2 Experimental results

2.2.2.1 Dielectric dispersion of the films II

The values of ε'and ε'' of films I and II in the frequency range below 10^4 Hz are quite close to each other. The main difference between the permittivity's spectra of these films observed in the frequency range higher of 10^5 Hz

In this frequencies region permittivity spectra of the films II reveal sharp decrease in ε' while the dielectric losses of ε'' has a form of enough narrow peak (see Figure 10). Such behavior of the spectrum is typical for the Debye dipole relaxation process, and will be discussed later.

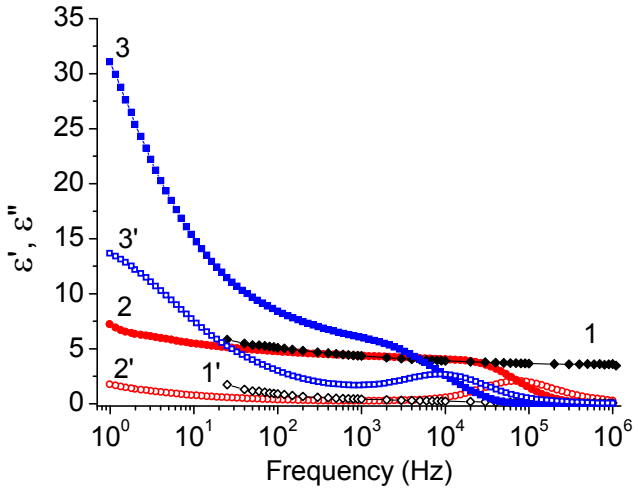

Fig. 10. The frequency dependence of ε 'and ε'' for: Film I: - (1 and 1'), Film II - (2, 2'), Film III - (3, 3').

2.2.2.2 Dielectric dispersion of the films III

The ε (ω) spectra of the films III, similar to those of the films II, but for the films III decreasing of ε 'is observed in the frequency of large 10^4Hz. The frequency at which a maximum of dielectric loss ε'' observed in films III, is $\nu_{max} \approx 9{,}7 \cdot 10^3$ Hz, while for films II, this frequency is $7{,}5 \cdot 10^4$ Hz (see Figure 10). At frequencies $\nu \leq 10^4$ Hz the magnitude of ε' of films III reveal a sharp increase with decreasing frequency of the external electric field and greatly exceeds the corresponding values of the films I and II.

2.2.2.3 AC conductivity of the films II and III

In contrast to the film I conductivity of the films II and III may be approximated by a power law $\sigma(\omega) \sim \omega^s$ on the frequency of the alternating electric field only in a very limited range of

frequencies. So for films II, this area is $1 \le \nu \le 4 \cdot 10^2$ Hz in which the exponent is 0.66, and for films III conductivity satisfactorily approximated by a power law with exponent s = 0,63 in the frequency range $5 \le \nu \le 5 \cdot 10^2$ Hz.

For both types of films, a significant increase of the growth rate of the conductivity is observed at frequencies exceeding $2 \cdot 10^3$ Hz, however, the conductivity of the films II and III begins very weakly dependent on frequency of external electric field (see Figure 11) at frequencies larger of 10^5 and $3 \cdot 10^4$ Hz respectively.

The conductivity of films III containing tetraaniline exceeds the conductivity of the films II in the frequency range $1 \le \nu \le 3 \cdot 10^4$ Hz ,while at higher frequencies observed the opposite picture in which the conductivity of the films II is higher then that of films III (see the same figure).

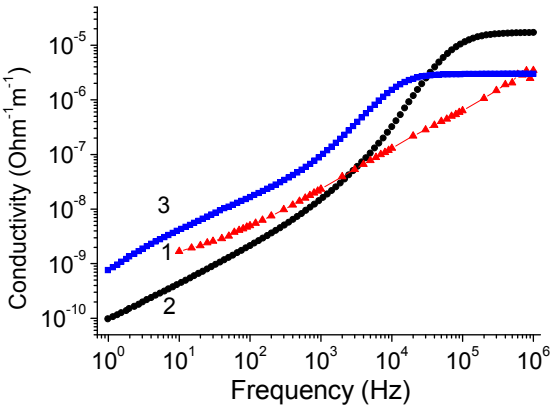

Fig. 11. Frequency dependence of AC conductivity of: films I - (1), film II - (2) and film III - (3)

2.3 Discussion

2.3.1 Ellipsometry of films I

Analysis of ellipsometric spectra shows that the value of ε' of the *nc*-Si films under study varies in the range of 2.1–1.1 in the energy range of 2–4.4 eV or in the frequency range of 5×10^{14} – 1×10^{15} Hz of the electromagnetic field, respectively, which is significantly below the values typical of *c*-Si in this range. In our opinion, there are two causes resulting in such low ε' and ε''. One is that *nc*-Si particles contacted with atmospheric oxygen for some time during film preparation; therefore, their surface was coated with a SiO_x + SiO_2 layer ($0 \le x \le 2$). Silicon nanoparticles oxidation was studied by Schuppler at al. (Schuppler at al., 1995), in that study the SiO_x layer thickness on their surface was determined as a function of the nanoparticle diameter. It was shown that the SiO_x + SiO_2 layer thickness in the nanoparticle diameter range of 10–3 nm is ~1 nm. However, this means that the ratio of the volume of the crystalline silicon core to the volume of the SiO*x* amorphous shell is from 100 to 40%. In

other words, the oxidized crystalline silicon nanoparticle with a size smaller than 10 nm should exhibit amorphous properties to an appreciable extent. We have confirmed this statement previously based on an analysis of Raman spectra of *nc*-Si thin films (see section 2.A.2.1 and also Dorofeev at al., *2009*). The second cause of a decrease in the permittivity is air gaps between nanoparticles, which appear during film formation.

To estimate the relation between crystalline and amorphous film components and their porosity, we use the Bruggeman EMA model. In the EMA approximation, the effective permittivity of the inhomogeneous medium consisting of spherical microobjects with permittivities ε_1, ε_2, …,ε_{N-1}, immersed into a medium with ε_N ($\varepsilon_N \equiv \varepsilon_e$) is determined from the equation

$$\sum_{i=1}^{N} f_i \frac{(\varepsilon_i - \varepsilon_e)}{(\varepsilon_i + 2\varepsilon_e)} = 0 \quad \sum_{i=1}^{N} f_i = 1 \tag{5}$$

where: $f_i = \dfrac{V_i}{\sum_{i=1}^{N} V_i}$

is the degree of medium volume filling with an element with permittivity ε_i and V_i is the volume occupied by this element.

Initially, to determine ε_e of the films under study, we assumed that the medium is two-phase and consists of purely crystalline silicon nanoparticles and the air gaps. In this case, Eq. (5) was reduced to a sum of two terms; knowing the dispersion relation of crystalline silicon, it was required to determine f_1 and f_2 so that approximating dispersion profiles would be identical to experimental $\varepsilon'(\nu)$ and $\varepsilon''(\nu)$. However, it was impossible to achieve satisfactory approximation at no values of f_1 and f_2.

Since the oxidation state of nanoparticles is unknown, we assumed that each particle in the two phase Bruggeman model behaves on average as a SiO_x medium (rather than as crystalline silicon), where $0 \le x \le 2$ was a fitting parameter, as well as f_1 and f_2. The $\varepsilon'(\nu)$ and $\varepsilon''(\nu)$ spectra for SiO_x in the entire range $0 \le x \le 2$ were taken from (Zuter, 1980), in which it was supposed that SiO_x is a mixture of $Si–Si_yO_{4-y}$ tetrahedra; the random parameter takes values from 0 to 4 (random binding model (Hubner, 1980)). Using these spectra, it became possible to achieve good approximation of the experimental dependences $\varepsilon'(\nu)$ and $\varepsilon''(\nu)$ at $x = 1$ and $f_1 = f_2 = 0.5$. The approximating EMA spectra for these parameters are shown in Fig. 5 by dashed curves. Thus, it was shown that the *nc*-Si films under study on average behave as media consisting of SiO with a porosity of 0.5. Here we note already mentioned study (Pickering, 1984) in which the $\varepsilon'(\nu)$ and $\varepsilon''(\nu)$ spectra were measured and which are qualitatively and quantitatively rather similar to the spectra analyzed in the present study.

The absorption spectra of *nc*-Si films calculated from ellipsometric data are quite typical. As seen in Fig. 6, the film absorption at incident photon energies below 3 eV is stronger than that of *c*-Si; at higher energies, it is significantly lower. Such an absorption behavior shows that the SiO_x shell with high density of states of defects near to the phase interface with the crystalline core mainly contributes to absorption for low energy photons; photons with

energies above 3 eV are mostly absorbed by crystalline cores of nanoparticles with a wider band gap than that of *c*-Si due to quantum confinement.

2.3.2 Frequency dependence of the capacitance of films I

There are several models of the interpretation of the results of measurements of the ac conductivity of materials. For semiconductors, the model of (Goswami,A. & Goswami,A.P. 1973) is a good approximation, according to which a conductive material is a composition of a capacitor with capacitance C_1 and a resistor with conductance G_1 ($G_1 = 1/R$) connected in parallel. Furthermore, to take into account the effect of supplying contacts, a resistor with conductance G_2 ($G_2 = 1/r$) is connected in series with this group. According to this model, C_1 and G_1 are independent of the frequency of the applied ac electric field; however, G_1 depends on the conductive material temperature.

If the sample capacitance is measured in the mode of in parallel connected *Cp*, the measured value is related to C_1, G_1, and G_2 as

$$C_p = \frac{C_1 G_2^2}{\left(G_1 + G_2\right)^2 + \left(2\pi\nu C_1\right)^2}$$

We can see from this equality that the measured *nc*-Si film capacitance should satisfy the condition $Cp \sim \nu^{-2}$ while satisfying the conditions of the model of(27Goswami,A. & Goswami,A.P. 1973). However, it was impossible to approximate the experimental curve for $C_{nc\text{-Si}}$ shown in Fig. 7 by such power law dependence. Such a fact suggests that C_1 and G_1 should depend on frequency. Indeed, under experimental conditions, $G_2 >> G_1$ and $G_2 >> \nu C_1$, hence, $Cp \approx C_1$.

Therefore, for approximation, we used the following semi empirical function:

$$C_{nc-Si}(\nu) = C_\infty + \frac{C}{1 + \left(A\nu\right)^\beta} \tag{6}$$

It follows from formula (6) that $C_{nc\text{-Si}} \to C_\infty$, at $\nu \to \infty$ and $C_{nc\text{-Si}} = C_\infty + C \equiv C(0)$ at $\nu = 0$.

Thus, the quantity C_∞ entering expression (6) is the film capacitance at an "infinitely high frequency" and $C(0) = C_\infty + C$ is the film static capacitance. The dimension of the fitting parameter *A* in the formula is time; the fitting parameter β defines the power law dependence of $C_{nc\text{-Si}}$ on the applied ac field frequency. Function (6) appeared to be a very good approximation of the experimental dependence $C_{nc\text{-Si}}(\nu)$ at the following coefficients: $C_\infty = 3.9 \times 10^{-10}$ F, $C(0) = 11.8 \times 10^{-10}$ F, $A = 0.5$, and $\beta = 0.32$.

The film capacitance is related to the real component of its permittivity by the relation $C_{nc\text{-Si}}(\nu) = \varepsilon'_{nc\text{-Si}}(\nu) \cdot C_0$. As noted above, $C_0 = 1.15 \times 10^{-10}$ F for the film under study; the static and optical permittivities $\varepsilon_s = \varepsilon(0) = 10.3$ and $\varepsilon_\infty = 3.4$ correspond to the determined capacitances $C(0)$ and C_∞.

The static permittivity of the film under study, which is 10.3, is significantly lower than the permittivity of crystalline silicon, which, as is known, is ~ 12. This result will be discussed below.

2.3.3 Dielectric relaxation in films I

The ε'(ν) and ε''(ν) frequency spectra obtained by measuring the *nc*-Si film impedance are shown in Fig. 8. The semi empirical Cole–Cole relation (Cole, K. S. & Cole, R. H., 1941; Moliton, 2007) appeared to be a good approximation for these spectra,

$$\varepsilon = \varepsilon_\infty + \frac{\varepsilon_s - \varepsilon_\infty}{1 + (i\omega\tau)^{1-h}} \quad 0 \le h \le 1 \tag{7}$$

where ε_s and ε_∞ are the static and optical permittivities determined above, $\omega = 2\pi\nu$ is the cyclic frequency, and τ is the dipole relaxation time.

As is known, the Cole–Cole relation is valid when a material simultaneously contains several types of dipoles each with a specific relaxation time. Therefore, the quantity τ entering Eq. (7) is the relaxation time averaged over the ensemble of dipole groups contained by the *nc*-Si film under study.

The approximating Cole–Cole curves are shown in Fig. 8.a by dashed curves. We can see that ε'(ν) is very well approximated in the entire measured frequency range; for ε''(ν), the Cole–Cole dependence exhibits good agreement only in the frequency range of $2 \times 10^2 \le \nu \le 10^6$ Hz. The values $\varepsilon_s = 10.8$, $\varepsilon_\infty = 3.43$, $\tau = 6 \times 10^{-2}$ s, and $h = 0.7$ correspond to the found approximation. It should be noted here that the value of ε_∞ is close to the values of ε' determined in the optical region by the ellipsometry method.

A comparison of the values of ε_s and ε_∞ corresponding to the Cole–Cole approximation with similar values determined from capacitance measurements shows the closeness of their numerical values. The value of $1 - h$ is also very close to the exponent β in formula (6). Furthermore, if we consider that A in formula (6) is the relaxation time multiplied by 2π, then $\tau = A/2\pi = 6.4 \times 10^{-2}$ s, which is also close to the average dipole relaxation time corresponding to the Cole–Cole approximation.

The static permittivity $\varepsilon_s = 10.8$ determined from the Cole–Cole relation is slightly larger than the similar value found from Eq. (6); however, it is also smaller than $\varepsilon_s = 12$ characteristic of crystalline silicon.

In our opinion, there are two causes resulting in a decrease in ε_s for the *nc*-Si film in comparison with ε_s of *c*-Si. The first cause is associated with air voids in the film body; the second cause is that the size distribution of nanoparticles composing the film includes a large fraction of particles with sizes smaller than 10 nm (see the Fig. 1). In (Tsu at al., 1997), the permittivity of silicon nanoparticles was calculated as a function of their size. According to these results, the static permittivity decreases as the particle diameter becomes smaller than 10 nm; for particles 10 nm in diameter, the permittivity is from 11.2 to 10.1, depending on the used calculation model.

In Fig. 8.a, in the frequency region $\nu \le 2 \times 10^2$ Hz, we can see a notable disagreement between the Cole–Cole approximating function and the experimental dependence ε''(ν). This disagreement is caused by the fact that the Cole–Cole relation that describes dipole moment relaxation in dielectrics does not take into account the presence of free electric charges. However, free charges exist in the *nc*-Si film under study, which is indicated by the nonzero dc conductivity, which, as noted above, is $\sigma(0) = 9 \times 10^{-10}$ Ω^{-1} m^{-1} at temperature $T = 297$ K.

According to studies by Barton, Nakajima, and Namikawa (Barton 1966; Nakajima, 1972; Namikawa, 1975), the frequency ν_m corresponding to the dispersion maximum for $\varepsilon''(\nu)$ is related to $\sigma(0)$ as $\sigma(0) = p(\varepsilon_s - \varepsilon_\infty).\varepsilon_0 2\pi\nu_m$, where the numerical coefficient p is approximately equal to unity. We can see in Fig. 8.a that the Cole–Cole approximating function reaches a maximum at the frequency ν_m = 2.5 Hz, and this value is in good agreement with the experimental value of $\sigma(0)$ when using the Barton–Nakajima–Namikawa formula.

To take into account the conductivity associates with free electric charges, relation (4) should be written as

$$\varepsilon = \varepsilon_\infty + \frac{\varepsilon_s - \varepsilon_\infty}{1 + (i\omega\tau)^{1-h}} + \frac{\sigma(0)}{\varepsilon_0 \omega} \tag{8}$$

The approximation of the $\varepsilon''(\nu)$ spectrum of the film under study is shown by the dashed curve in Fig. 8.a (curve *5*), from which it is obvious that function (8) is a good approach of the experimental dependence $\varepsilon''(\nu)$.

The effect of free electric charges on dielectric properties of the *nc*-Si film rather clearly appears in the Nyquist plot in which ε'' for each frequency is shown as a function of ε' (see Fig. 8.b).

It follows from the Cole–Cole approximation (see curve *2* in Fig. 8.b) that the $\varepsilon''(\varepsilon')$ should be shaped as a part of a semicircle whose center is below the horizontal axis ε''. The intersection of this circle with the ε' axis at $\omega = 0$ and $\omega \to \infty$ yields the values of ε_s and ε_∞.

Figure 8.b shows only the semicircle part corresponding to the measured frequency range; therefore, the value ε_s = 10.8 is out of sight of the figure; the intersection of the semicircle with the ε' axis at $\omega \to \infty$ is clearly seen and corresponds to ε_∞ = 3.4. The same figure shows the approximation corresponding to function (8) (curve *3*), similar to the approximation shown in Fig. 8.a.

2.3.4 AC conductivity of films I

To determine the nature of electric charge transport in *nc*-Si films, the frequency dependence of the conductivity $\sigma_{AC}(\nu)$, $\sigma_{AC}(\nu) - \sigma(0) = \varepsilon_0 \cdot 2\pi\nu \cdot \varepsilon''(\nu)$, was studied.

The $\sigma_{ac}(\nu)$–$\sigma(0)$ plot on a log scale for the film analyzed in this paper is shown in Fig. 10. We can see that $\sigma_{AC}(\nu)$ in the entire measured frequency range is well approximated by the power law function: $\sigma_{ac}(\nu) = \sigma(0) + A\nu^s$ with s = 0.74. Such $\sigma_{AC}(\nu)$ behavior means that the electric transport in the film has the hopping mechanism, which in turn is a manifestation of the structure disorder in that film region over which charge transport occurs.

Currently, there are several theoretical models describing hopping conductivity in unordered solids. All these models yield the power law dependence of the ac conductivity on the ac electric field frequency:$\sigma(\nu) \sim \nu^s$. However, the numerical values of the exponent s differ. For example, in the models (Austin & Mott, 1969; Hunt, 2001) according to which the conduction results from electric charge tunneling through energy barriers separating close localized states, the parameter s is given by

$$s = 1 + q \times \ln^{-1}\left(\frac{\nu}{\nu_{ph}}\right) \tag{9}$$

where q = 4 or 5, depending on the theoretical model, and $\nu_{ph} \approx 10^{12}$ Hz is the phonon frequency.

It follows from relation (9) that s should decrease with frequency. However, such behavior of s contradicts our experimental data and a large number of other experimental data (Dyre & Schrøder, 2000).

Currently, it has been sufficiently reliably determined that a large role in conduction processes in unordered solids is played by percolation processes with the result that electric transport occurs along trajectories with the lowest resistance (percolation trajectories) (Hunt, 2001; Isichenko, 1992). Conductive properties of percolation trajectories are controlled by the structure of (percolation) clusters composing the shell of solids.

In highly unordered solids, percolation trajectories at small scales exhibit a fractal structure with the result that their fractal dimension d_f appears larger than the topological one D (e.g., the fractal and topological dimensions of the Brownian particle trajectory is $d_f = 2$ and $D = 1$) (Isichenko, 1992).

In this regard, we note theoretical studies (Dyre & Schrøder, 2000; Schrøder & Dyre, 2002; Schrøder & Dyre, 2008) in which the diffusion cluster approximation (DCA) model is formulated. As these papers, it is argued that the so-called diffusion clusters with fractal dimensions of 1.1–1.7 make the largest contribution to the ac conductivity in the percolation mode. This statement means that the fractal structure of such clusters is simpler than the structure of multiply connected percolation clusters formed above the percolation threshold in conductive materials (backbone clusters), the fractal dimension of which is 1.7 (Isichenko, 1992). Simultaneously, the structure of diffusion clusters is more branched than the network of singly connected clusters and breaking of each results in disappearance of the current flowing through it (*redbonds*). The fractal dimension of *redbonds* clusters is 1.1 (Isichenko, 1992).

In these papers, the universal dependence of the dimensionless complex conductivity

$$\tilde{\sigma} = \frac{\sigma_{AC}(\nu) + i\sigma''(\nu)}{\sigma(0)}$$

on the dimensionless frequency

$$\tilde{\omega} = \frac{\varepsilon_0\left(\varepsilon_s - \varepsilon_\infty\right)}{\sigma(0)} 2\pi\nu$$

was derived. This dependence is given by

$$\ln\tilde{\sigma} = \left(\frac{i\tilde{\omega}}{\tilde{\sigma}}\right)^{\frac{d_f}{2}} \tag{10}$$

The fractal dimension d_f in formula (10) is a fitting parameter. Processing of a large number of experimental dependences in (Schrøder & Dyre, 2002; Schrøder & Dyre, 2008) showed that the best agreement in the frequency region ν > 1 Hz is achieved at d_f = 1.35.

We compared the experimental dependence σ_{AC} (ν) obtained in the present study with the values defined by formula (10). Here it should be noted that complex valued equation (10) has no analytical solution and should be solved numerically.

However, in the low frequency region ω → 0, Eq. (10) can be written as $\tilde{\sigma} - 1 = (i\tilde{\omega})^{\frac{d_f}{2}}$; accordingly (Kononov at al., 2011):

$$\sigma_{AC}(\nu) - \sigma(0) = \sigma(0)^{\left(1-\frac{d_f}{2}\right)} \cos\left(\frac{\pi d_f}{4}\right)(2\pi\varepsilon_0\Delta\varepsilon)^{\frac{d_f}{2}} \nu^{\frac{d_f}{2}} \quad (11)$$

where $\Delta\varepsilon = \varepsilon_s - \varepsilon_\infty$.

Substitution of experimentally determined values of ε_s, ε_∞, σ(0), and $s \equiv d_f/2 = 0.74$ into formula (11) gives the approximating dependence for σ_{ac}(ν) (see Fig. 9) corresponding to the DCA model. We can see that the calculated dependence rather well approximates the experimental curve σac(ν) in the entire measured frequency range. At the same time, the calculated dependence yields values of σ_{AC} larger than the experimental ones by a factor of ~1.5. We attribute such disagreement to possible errors when determining the numerical values of ε_s, ε_∞, and σ(0).

2.3.5 Proton conductivity of films I

One of the possible causes that can result in σ(0) measurement errors for nc-Si films is the dependence of σ(0) on the ambient air humidity. We qualitatively determines the following systematic feature: the higher the laboratory air humidity, the higher (at a constant temperature) the conductivity σ(0) of films similar to the film analyzed in this paper. On the contrary, if the film is preliminarily heated at a temperature of ~200°C for a time longer than 15 min and then it is cooled to its initial temperature, the film conductivity will decrease almost by two orders of magnitude. Thus the presence of water in an atmosphere surrounding the film changes its conductive properties significantly. In (Nogami & Abe, 1997; Nogami at al., 1998) a similar phenomenon was observed in the study of the ionic conductivity in fused silica glasses. It was shown that, in the presence of Si–O–H bonds on the glass surfaces, H_2O molecules form complexes with them, confined hydrogen bonds. These complexes can dissociate forming free H_3O^+ ions and bound Si–O– groups according to the scheme:

$$\text{Si-O-H}\cdots\text{OH}_2 \rightarrow \text{Si-O}^- + \text{H}^+ : \text{H}_2\text{O}$$

Here, dots denote the hydrogen bond between H and O atoms. In this case, the dissociated proton H+ can be trapped by a neighboring H_2O molecule,

$$\text{H}_2\text{O}: \text{H}_2\text{O}_{(1)}:\text{H}^+ + \text{H}_2\text{O}_{(2)} \rightarrow \text{H}_2\text{O}_{(1)} + \text{H}^+ + \text{H}_2\text{O}_{(2)} \rightarrow \text{H}_2\text{O}_{(1)} + \text{H}^+ : \text{H}_2\text{O}_{(2)} \text{ etc.}$$

Such a scheme allows implementation of proton transport near the glass surface. Returning to nc-Si films, we note that particles used to apply films represent hydrogenized nanocrystalline silicon. However, when exposing these particles to atmospheric air, a SiO_x shell ($0 \le x \le 2$) is formed on their surface. In (Du at al., 2003; Cao at al., 2007), the kinetics of the interaction of H_2O molecules with SiO_2 chain structures was calculated. It was shown that H_2O molecules very efficiently break Si–O–Si bonds during the interaction with SiO_2 surface groups with the formation of Si–O–H groups. The subsequent interaction of H_2O molecules and Si–O–H groups yields H_3O^+ ions, which, having high mobility, can appreciably contribute to the proton transport along the SiO_2 chain.

In addition to the above process, the collective proton conductivity caused by associated Si–O–H groups, i.e., groups linked by hydrogen bond, as shown in Fig. 12.a (Glasser, 1975). Arrows in the diagram indicate the direction of positive charge transport.

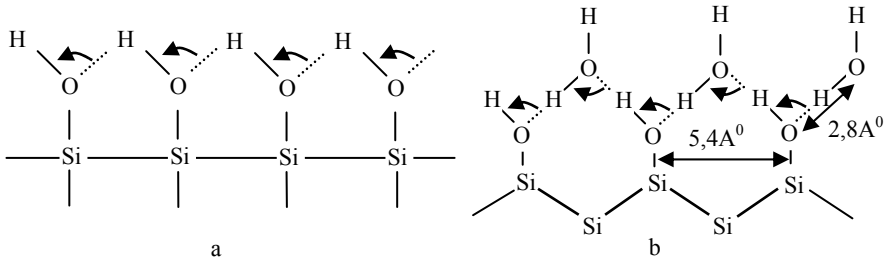

Fig. 12. Diagrams illustrating the mechanism of the collective proton conductivity, caused by (a) associated Si–O–H groups and (b) the interaction of water molecules with hydroxyl groups. Arrows indicate the direction of positive charge transport.

The collective proton conductivity is also possible during the interaction of water molecules with hydroxyl groups, which results in the surface structure shown in Fig. 12.b. Since the O···H—O group length is within 2.5–2.9 Å (Leite at al., 1998) and the angle between H–O–H bonds is ~104°, there is good spatial alignment between the element of this surface structure and the crystalline silicon lattice constant which, as is known, is 5.4 Å.

As applied to the nc-Si films analyzed in this paper, there is direct proof of the existence of such structures. Previously, in the investigations of IR transmission spectra of thin wafers (with thickness ≈50 μm) made by pressing ($P \sim 10^9$ Pa) from nc-Si powders similar to those used in this study, it was shown that the spectra contain a broad intense band with a maximum at ~3420 cm^{-1} (see Fig. 13 and Kononov at al., 2005). In papers (Wovchko at al., 1995; Stuart, 2004) this band is attributed to O–H vibrations in hydrogen bound hydroxyl groups. It was also shown that heating of nc-Si particles to 400°C causes an appreciably decrease in the intensity of the band near 3420 cm^{-1} and an increase in the intensity of the narrow band with a maximum near 3750 cm^{-1}, which is identified with

O–H vibrations in the isolated Si–O–H group (Kononov at al., 2005). Similar spectra are shown in Figure 13. Such behavior of the intensities of bands at 3420 and 3750 cm^{-1} means that associated Si–O–H groups become isolated upon heating of nc-Si particles. Accordingly, heating should decrease the proton conductivity associated with these groups.

Thus the dependence of the conductivity σ(0) of the *nc*-Si films under study on the ambient air humidity and the thermal behavior of the absorption bands associated with Si–O–H groups allows the conclusion to be drawn that the proton conductivity makes the main contribution to the dark dc conductivity of *nc*-Si films.

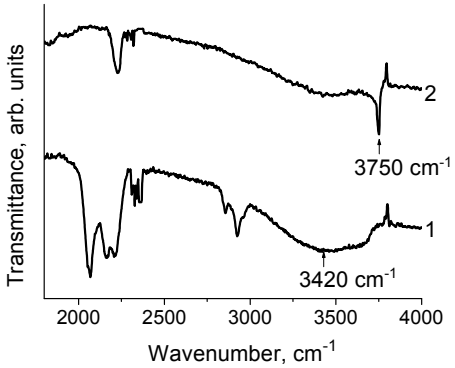

Fig. 13. Infrared transmittance spectra of: (*1*) - thin wafer from *nc*-Si particles prepared at a pressure of 5×10^8 Pa at 20^0C, (2) - the same *nc*-Si wafer but annealed at 400°C for 30 min.

2.3.6 Double dielectric relaxation in the films II and III

Earlier, we noted that the spectra of the ε′(ν) and ε″(ν) of the films II and III near a frequency ≈ 10^4 Hz reveal the structure arising in the Debye dipole relaxation. Following this observation for the numerical approximation of the experimental spectra, we used not only semi-empirical law of Cole-Cole, but the law of Debye dipole relaxation. Thus, all experimental spectra were approximated by the following relation:

$$\varepsilon = \frac{\varepsilon_S - \varepsilon_\infty}{1 + (i\omega\tau_1)^{1-h}} + \frac{\varepsilon_\infty}{1 + (i\omega\tau_2)^2} + \frac{\sigma(0)}{\varepsilon_0 \omega} \tag{12}$$

Here τ_1 and τ_2 is the relaxation times of dipole moments in the various structural components of the films. With the help of equation (12) was able to accurately approximate the dielectric spectra of the films studied; example of such an approximation for film II is shown in Figure 14.

Furthermore the approximation (12) allowed us to determine the static (ε_0), high-frequency (ε_∞) dielectric constants (ν ~ 10^5 Hz), the conductivity of the films at constant current σ (0), and relaxation times τ_1 and τ_2.

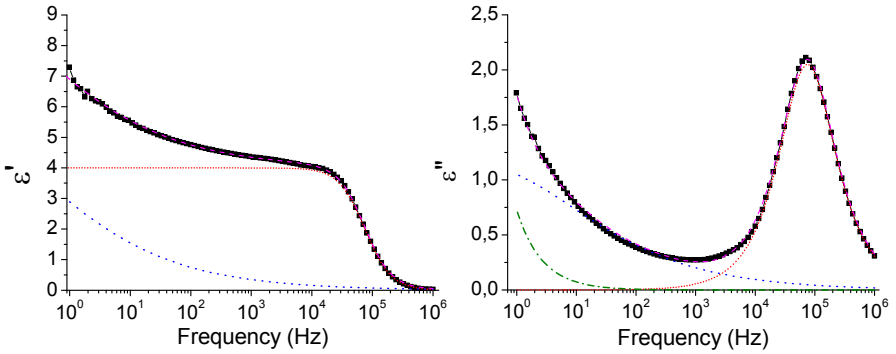

Fig. 14. Spectra of the real (a) and imaginary (b) components of permittivity film II. Short-dotted line shows the approximation of the Debye. Dotted line shows the approximation of the Cole-Cole. The dash-dotted line shows the approximation of free charges. The dashed line shows the complete approximation of the spectra.

№	ε_0	ε_∞	h	$\sigma(0)$, $(Ohm \cdot m)^{-1}$	σ_{DC}, $(Ohm \cdot m)^{-1}$	$\sigma_B(0)$, $(Ohm \cdot m)^{-1}$	τ_1, s	τ_2, s
I	10,8	3,4	0,74	$1{,}4 \cdot 10^{-9}$	$9 \cdot 10^{-10}$	10^{-9}	0,06	-
II	11,5	4	0,66	$4 \cdot 10^{-11}$	$3{,}5 \cdot 10^{-11}$	$9 \cdot 10^{-11}$	0,72	$2{,}12 \cdot 10^{-6}$
III	66,9	4,9	0,5	$9 \cdot 10^{-11}$	$3{,}5 \cdot 10^{-9}$	$2 \cdot 10^{-9}$	0,27	$1{,}75 \cdot 10^{-5}$

Table 1. Fit parameters for the two dielectric relaxation lows of the films investigated in this study. σ_{DC} and $\sigma_B(0)$ - the conductivites at constant current received from direct measurements of the films resistance and from the Barton–Nakajima–Namikawa formula.

These values for films I, II and III are shown in the table 1. The table 1 also gives values of $\sigma(0)$ received from direct measurements of the films resistance at constant current at T = 297K, and those which obtained from the Barton–Nakajima–Namikawa formula. From table 1 it can be seen that the values of the static dielectric constant of films III are about 67, significantly higher than similar values of the films I and II, which are close to the values characteristic of crystalline silicon. However, the value of $\varepsilon_0 \approx 67$ is much lower quantities $\varepsilon_0 \sim 10^3$ typical for composites consisting of nanoparticles of tin dioxide and polyaniline which have been reported in (Kousik at al., 2007)

The authors of this work attributed so high ε_0 to an anomalously strong polarization of nanoparticle of SnO_2 which caused by inhomogeneity of the conductivity of its surface and core. However, the value of $\varepsilon_0 \approx 67$ which have been measured by us, is quite close to the values of the static dielectric constant of tetraaniline with different degrees of doping it with hydrochloric acid (Bianchi at al., 1999) and which, depending on the degree of doping lies in the range 35 - 80.

The presence in equation (12) two different laws of approximation indicates that there are two different dipole relaxation process associated with the various structural components of

the studied films II and III. Very clear in understanding this phenomenon is a plot of ε'' vs ε '(Nyquist Plot), shown in Figure 15.

In the inset of Fig. 15 we can see that the dependence of ε'' vs of ε' for film III consists of two semicircles, which can be termed as high- and low- frequency components. The film II has a similar structure while the graph ε''(ε') of the film I consists of only one semicircle (which is a low-frequency component) and low-frequency tail defined by the presence of free charges. Nanoparticles of silicon used for deposition of films II and III were in ethanol for two years after their synthesis, i.e., they were subjected to natural oxidation significantly longer than the nanoparticles of which consist film I. Therefore we can assume that oxidation of their surface is significantly higher than that of nanoparticles films I.

The previous sections have shown that the optical and electrical properties of films I greatly influenced by the surface of the nanoparticles from which these films are composed. It was found that the average properties of the surface similar to those of SiO and the component ε (ω) is determined by the Cole-Cole law related to the dipole relaxation in SiO_x shell of silicon nanoparticles.

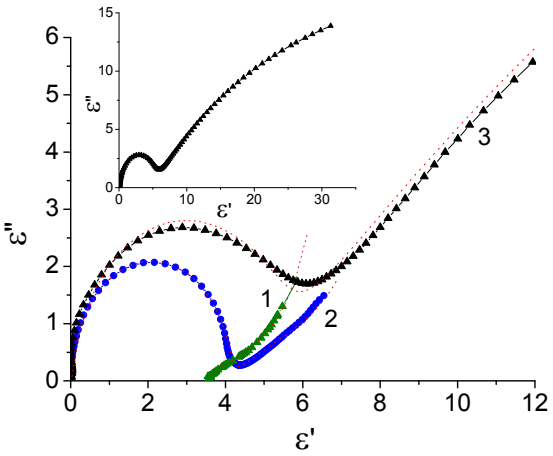

Fig. 15. The graph of dependence ε'' vs ε' for: film I - (1), film II - (2) and film III - (3)
The inset shows an expanded plot ε''(ε ') for film III.

Since during the aging process of silicon nanoparticles the SiO_2 shell must increase, the appearance of high-frequency components of the Debye spectra ε (ω) of the films II and III gives reason to assume that the source of this component is the structure of SiO_2 with a narrow distribution of the dipole, which was formed on the surface of nanoparticles in two years of their presence in ethanol.

The fact that the Debye component of the spectrum ε (ω) as well as component Cole-Cole connected with the surface of the nanoparticles is confirmed by the fact noted earlier that the maxima of the Debye peak in the spectra of ε''(ω) of the films II and III correspond to different frequencies ν_m.

The grains of silicon nanoparticles constituting the films II and III are similar to each other, so this difference frequency ν_m can be attributed only to differences in the strength of interaction between the dipoles on the surface of the nanoparticles in these films. In other words, the presence of tetraaniline complexes on the surface of silicon nanoparticles leads to a weakening of the interaction between the dipoles are formed on the surface at the polarization of the particle.

2.3.7 AC conductivity of the films II and III

Dependence of the conductivity of the films I, II and III of the frequency of the applied electric field is shown in Figure 11. This figure shows that the conductivity of films I with good accuracy obey the law:

$$\sigma(\omega) = \sigma(0) + A\omega^s. \tag{13}$$

In the entire range of measured frequencies, the exponent s = 0,74 equal to the value h which obtained from the approximation of the Cole-Cole and given in table 1.

Conductivity of the films II describe such an equation is possible only in very limited region, namely in the frequency range $\nu \le 10^3$Hz (let's call it a low-frequency component).

For low-frequency component of the conductivity of the films II as well as for the film**s** I, the value of s coincides with that of h, shown in Table 1. For films of III this statement is incorrect. Indeed, as noted in Section B.2 conductivity of the films III is well approximated by a power law exponent with s = 0,63 only in small range of frequencies $5 \le \nu \le 5 \cdot 10^2$ Hz. As can be seen from Table 1, this value differs significantly from the values of h = 0,5 obtained from the approximation of the Cole-Cole.

The coincidence of the values of s and h for a film I is explained as follows circumstance. Spectrum $\varepsilon''(\omega)$ of the film over the entire range of measured frequencies is approximated by the Cole-Cole distribution which has the form:

$$\varepsilon'' = \frac{A(\omega\tau_1)^{1-h}}{1 + B(\omega\tau_1)^{1-h} + (\omega\tau_1)^{2(1-h)}} = \left(\frac{A}{B + \frac{1}{(\omega\tau_1)^{1-h}} + (\omega\tau_1)^{1-h}} \right)$$

Where A and B is constants and B≤2

If $\omega\tau_1 >> 1$, this equation takes the form: $\varepsilon'' \approx \frac{A}{(\omega\tau_1)^{1-h}}$,

and hence the following relation is valid for the conductivity $\sigma(\omega) - \sigma(0) = \varepsilon_0 \cdot \omega \cdot \varepsilon'' \sim \omega^h$

As can be seen from Table 1 for the film I τ_1 = 0,06 s, hence equation (13) is valid for it, at frequencies $\nu \ge 10$ Hz. A similar analysis is applicable also to the low frequency component of the film II. For film II τ_1 = 0,72 s, therefore, the dependence (13) will be observed if $\nu \ge 1$ Hz. This fact is shown in Figure 16, where the conductivity of the films II and III is approximated by the sum of σ (0) and two distributions of Cole-Cole and Debye.

From this figure it is clear that if the ε''(ω) spectrum of the films II describes only the distribution of the Cole-Cole, they would obey the conductivity relation (13) throughout the frequency range $1 \le \nu \le 10^6$ Hz as well as the conductivity of the films I.

For the film III observed more complicated situation, its spectrum is distorted with respect to relation (13), not only at high frequencies $\nu \ge 10^3$Hz, but also at frequencies $\nu \le 10$ Hz (see Figure 16, b). According to the vast majority of experimental data, the frequency dependence of the conductivity of disordered media has kind of plateau (low-frequency plateaus) at low frequencies and is a power in excess of a certain critical frequency.

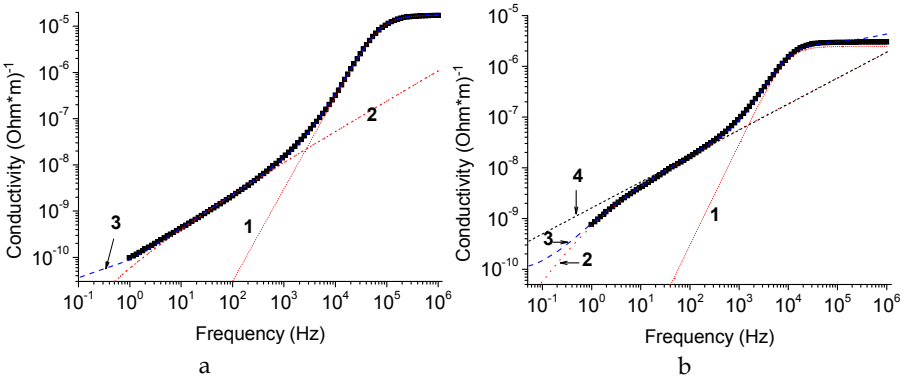

Fig. 16. The frequency dependence of AC conductivity of the films II (a) and III (b), as well as its approximation by: the Debye law - (1), the relation of Cole - Cole - (2) and the total approximation, which takes into account the dc conductivity - (3). (4) - power dependence with an exponent equal to the value of h at the Cole-Cole relation.

For films of III observes the opposite situation, instead, the appearance of a plateau at low frequencies, the conductivity σ (ω) begins to decrease more quickly with decreasing frequency of the external electric field. The reason for the absence of such low frequency plateau may be the existence of significant resistance at the interface of the film-electrode.

Comparison of σ (0), σ_{DC} and σ_B (0) from Table 1 shows their good agreement for film I. For films II are in good agreement the values σ (0) and σ_{DC} but somewhat too high the value of σ_B (0) with respect to them. For films III good agreement is observed for the values σ_{DC} and σ_B (0) but σ (0) is less than these quantities is about 20 times. The fact that σ_{DCI} more than 25 times higher then σ_{DCII} (see Table1) confirms our earlier assumption that the degree of surface oxidation of silicon nanoparticles of films II is significantly higher than that in films I.

At frequencies $\nu_{s1} \ge 1 \cdot 10^5$Hz for films II and $\nu_{s2} \ge 3 \cdot 10^4$Hz for films III conductivity begins to depend very weakly on the frequency of an external electric field. This behavior is usually associated with the manifestation of the nature of hopping conduction (Barsoukov & Macdonald, 2002), and the frequency ν_c determined by the height of the barriers between potential wells, which are involved in the hopping transport of charge carriers. Because $\nu_{s1} > \nu_{s2}$, we can conclude that the presence of tetraaniline on the surface of silicon nanoparticles lowers the barriers separating localized states.

3. Conclusion

Dielectric and transport properties of thin films obtained by deposition of silicon nanoparticles from ethanol sols on a glass, quartz, and aluminum substrates were measured by optical ellipsometry and impedance spectroscopy methods. The real and imaginary permittivities of *nc*-Si films were measured in frequency ranges of 5×10^{14}–10^{15} and 10–10^6 Hz. It was found that the permittivity spectra depend on the time which has elapsed since the synthesis of nanoparticles until their deposition on the substrate.

Only one type of dipole relaxation, which can be described by semi-empirical Cole-Cole equation, exists in films prepared from sols with silicon nanoparticles, synthesized a week before their deposition on a substrate (film I). In films prepared from sols containing aged nanoparticles (film II) there is a double-dipole relaxation, which is revealed in the fact that for the approximation of the experimental spectra of these films not only Cole-Cole relation but the law of Debye dipole relaxation should be used. A similar confirmation is valid also for the films deposited from the sols with aged nanoparticles in which tetra aniline was added (film III).

In the measured frequency ranges, ε' and ε'' vary within 2.1–1.1, 3.4–6.2 and 0.25–0.75, 0.08–1.8, respectively. From the EMA analysis of the spectra, it was concluded that the *nc*-Si film in light reflection processes can on average be considered as a two component medium consisting of SiO and air gaps with a porosity of 50%.

It was shown that the complex dielectric dispersion of films in the frequency range of 10 – 2×10^6 Hz is well approximated by the semiempirical Cole–Cole relation, taking into account the effect of free charges controlling the dark dc conductivity of films.

An analysis of the frequency dependences of the ac conductivity of the studied films allowed the conclusion to be drawn that the ac conduction process is well described by the cluster diffusion approximation model.

The dependence of the dark conductivity of films on the ambient air humidity and the temperature dependence of absorption bands related to associated Si–O–H groups allows the conclusion to be drawn that the conductivity at frequencies lower than 2×10^2 Hz is controlled by proton transport through hydrogen bound hydroxyl groups on the surface of silicon nanoparticles.

Using Cole-Cole and Debye relations for approximation of experimental spectra $\varepsilon(\omega)$ the values of static permittivity ε_0 of films I, II and III have been found. For films I and II quantities ε_0 close to the values characteristic of crystalline silicon. For films of III $\varepsilon_0 \approx 67$, i.e. greatly exceeds ε_0 for c-Si. Such a high value ε_0 we attribute to increasing polarization of the silicon nanoparticles when the tetraaniline complexes are attached to their surface.

AC conductivity of the films II and III in the whole frequency range of 1-10^6 Hz can not be approximated by a power law, which is characteristic of the conductivity of the films I. We show that such deviation from the dependence $\sigma_{AS} \sim \omega^s$ is associated with a double-dielecrtic relaxation typical for films II and III and with the presence in the spectra $\varepsilon''(\omega)$ of these films Debye components.

4. Acknowledgment

We sincerely thank Dr. Helen Yagudayev, the senior researcher of the Shemyakin - Ovchinnicov Institute of Bioorganic Chemistry of RAS, for providing us the conductive tetraaniline solutions.

We also thank our colleagues prof. Plotnichenko V.G., prof. Kuz'min G.P., prof. Ischenko A.A., dr. Koltashev V.V., researcher Tikhonevich O.V. for the fruitful cooperation in investigation of the properties of nano-sized silicon.

5. References

[1] Anopchenko,A.; Marconi, A.; Moser, E.; Prezioso, S.; Wang; M., Pavesi; L., Pucker, G. & Bellutti. P. J. (2009) Low-voltage onset of electroluminescence in nanocrystalline-Si/SiO_2 multilayers *Journal of Applied Physics,* Vol.106, (2009), p.p. 033104, ISSN 0021-8979

[2] Aspens, D. E. & Studna, A. A. (1983) Dielectric functions and optical parameters of Si, Ge, Gap, GaAs, GaSb, InP, InAs, and InSb from 1.5 to 6.0 eV, *Physical Review* B, Vol. 27,№2, (January 1983), p.p.985 - 1009

[3] Austin, I. G. & Mott, N. F. (1069). Polarons in crystalline and non-crystalline materials. A*dvances in physics*, Vol.18, №71, (January 1969), pp. 41-102

[4] Axelrod, E.; Givant, A.; Shappir, J.; Feldman, Y. & Sa'ar. A. (2002) Dielectric relaxation and transport in porous silicon *Physical Review* B, Vol. 65, №16, (April 2002) , p.p. 165429(1-7) ,ISSN 0163-1829

[5] Azzam, R.M.A. & Bashara N.M. (1977) *Ellipsometry and polarized light*, North-Holland publishing company, ISBN 1704050000 , Amsterdam, New York, Oxford

[6] Barsoukov, E. & Macdonald, J. R. (2005) *Impedance Spectroscopy. Theory, Experiment, and Applications*, Second Edition, A John Wiley & Sons, Inc., Publication, New Jersey, USA and Canada ISBN: 0-471-64749-7

[7] J. L. Barton, (1966). *Verres Réfract*. Vol. 20, p.p. 328 (1966).

[8] Ben-Chorin, M.; Möller, F.; Koch, F.; Schirmacher, W. & Eberhard, M. (1995) Hopping transport on a fractal: ac conductivity of porous silicon *Physical Review* B, Vol. 51, №4, (January 1995) , p.p. 2199(1-15) , ISSN 0163-1829

[9] Bianchi, R.F.; Leal Ferreira, G.F.; Lepienski, C.M. & Faria, R.M. (1999). Alternating electrical conductivity of polyaniline. *Journal of Chemical Physics*, Vol.110,№9, (March 1999), p.p. 4602-4607, ISSN 0021-9606

[10] D.A.G. Bruggeman. (1935). Berechung verschiedener physikalisher konstanten von heterogenen substanzen. *Annalen der Physik* (Leipzig), Vol. 24, (1935), pp. 636-664

[11] Brus, L.E.; Szajowski, P.F.; Wilson, W. L.; Harris, T. D.; Schuppler, S. & Citrin. P. H. (1995) Electronic Spectroscopy and Photophysics of Si Nanocrystals: Relationship to Bulk c-Si and Porous Si. *Journal of American Chemical Society,* Vol. 117, (1995) pp. 2915-2922

[12] Campbell, I.H. & Faushet P.M. (1986) The effect of microcrystalline size and shape on the one phonon Raman spectra of crystalline semiconductors. Solid State Communications. Vol. 58, №10 (February 1986), p.p.739-741, ISSN 0038-1098

[13] Cao, Chao; He, Yao; Torras, J.; Deumens, E.; Trickey, S. B. & Cheng, Hai-Ping. (2007) Fracture, water dissociation, and proton conduction in SiO_2 nanochains. *Journal of Chemical Physics,* Vol. 126, №21, (June 2007) p.p. 211101(1-3), ISSN 0021-9606

[14] Cole, K. S. & Cole, R. H. (1941). Dispersion and Absorption in Dielectrics. *Journal of Chemical Physics,* Vol. 9, №, (February 1941) p.p. 341-351, ISSN 0021-9606

[15] Conte, G.; Feliciangeli, M. C.; & Rossi, M. C. (2006) Impedance of nanometer sized silicon structures. *Applied Physics Letters,* Vol. 89, № 2, (July 2006), p.p.022118(1-3), ISSN0003-6951

[16] Dorofeev, S. G.; Kononov, N. N.; Ishchenko, A. A.; Vasil'ev, R. B.; Goldschtrakh, M. A.; Zaitseva, K. V.; Koltashev, V. V.; Plotnichenko, V. G. and O. V. Tikhonevich. (2009). Optical and Structural Properties of Thin Films Precipitated from the Sol of Silicon Nanoparticles. *Rus. Semiconductors,* Vol. 43, No. 11, (April 2009), pp. 1420–1427. ISSN 1063-7826.

[17] Du, Mao-Hua; Kolchin, A. & Chenga, Hai-Ping. (2003). Water–silica surface interactions: A combined quantum-classical molecular dynamic study of energetics and reaction pathways. *Journal of Chemical Physics*, Vol. 119, №131, p.p.6418 – 6422 (2003) ISSN 0021-9606.

[18] Dyre, J.C. & Schrøder, T. B. (2000). Universality of ac conduction in disordered solids. *Reviews of Modern Physics*, Vol.72, №3, (July 2000), p.p. 873 – 892, ISSN 0034-6861.

[19] Ehbrecht, M.; Ferkel, H.; Huisken, F.; Holz, L.; Polivanov, Yu.N.; Smirnov, V.V.; Stelmakh, O.M. & Schmidt R. (1995) Deposition and analysis of silicon clusters generated by laser-induced gas phase reaction *Journal of Applied Physics,* Vol.78, № 9, (November 1995), p.p. 5302-5305, ISSN 0021-8979

[20] Glasser, L. (1975) Proton Conduction and Injection in Solids. *Chemical Reviews*, Vol.75, №1, (January 1974), p.p. 21 – 65.

[21] Goswami, A. & Goswami, A.P. (1973). Dielectric and optical properties of ZnS films. *Thin Solid Films* Vol. 16, (January 1973), p.p. 175 – 185

[22] Hubner, K. (1980). Chemical Bond and Related Properties of SiO_2. *Physica Status Solidi* (a) Vol. 61, (May 1980), p.p. 665-673

[23] Hunt, A.G. (2001). Ac hopping conduction: perspective from percolation theory. *Philosophical Magazine* B Vol. 64, №9, (2001), p.p. 875-913, ISSN 1364-2812 print/ISSN 1463-6417 online

[24] Isichenko, M. B. (1992) Percolation, statistical topography, and transport in random media. *Reviews of Modern Physics*, Vol. 64, №4, (October 1992), p.p.961 – 1043, ISSN 0034-6861.

[25] Jurbergs, D.; Rogojina, E.; Mongolini, L. & Kortshagen, U. (2006). Silicon nanocrystalls with ensemble quantum yields exceeding 60%. *Applied Physycs Letters,* Vol. 88, №23, (June 2006) 233116(1-3), ISSN 0003-6951.

[26] Kakinuma, H.; Mohri, M.; Sakamoto, M. & Tsuruoka T. (1991). Sructural properties of polycrystalline silicon films prepared at low temperature by chemical vapor deposition. *Journal of Applied Physics*, Vol.70, (December 1991), p.p. 7374 - 7381, ISSN 0021-8979

[27] Kononov, N. N.; Kuz'min, G. P.; Orlov, A. N.; Surkov, A. A. and Tikhonevich, O. V. (2005). Optical and Electrical Properties of Thin Wafers Fabricated from Nanocrystalline Silicon Powder. *Rus. Semiconductors,* Vol. 39, No. 7, (November 2005), pp. 835–839, ISSN 1063-7826

[28] Kononov, N. N.; Dorofeev, S. G.; Ishenko, A. A.; Mironov, R. A.; Plotnichenko, V. G. & E. M. Dianov. (2011). Dielectric and Transport Properties of Thin Films Precipitated from Sols with Silicon Nanoparticles *Rus. Semiconductors,* 2011, Vol. 45, No. 8, (August 2011), pp. 1038–1048. ISSN 1063-7826

[29] Kovalev, D.; Polisski, G.; Ben-Chorin, M.; Diener, J. & Koch F. (1996) The temperature dependence of the absorption coefficient of porous silicon *Journal of Applied Physics*, Vol.80, №10, (November 1996) , p.p.5978 -5983, ISSN 0021-8979

[30] Kousik, D. & De, S.K. (2007). Double dielectric relaxations in SnO_2 nanoparticles dispersed in conducting polymer. *Journal of Applied Physics,* Vol.102,.№ 8, (October 2007), p.p. 084110 -1,084110 -7, ISSN 0021-8979 print | 1089-7550 online

[31] Kuz'min, G.P.; Karasev, M.E.; Khokhlov, E.M. Kononov, N.N.; Korovin, S.B.; Plotnichenko, V.G.; Polyakov, S.N.; Pustovoy, V.I. & Tikhonevich O.V. (2000). Nanosize Silicon Powders: The Structure and Optical Properties. *Rus. Laser Physics* Vol.10, №4, (April 2000) p.p. 939-945

[32] Leite, V. B. P.; Cavalli, A. & Oliveira, O. N. Jr. (1998) Hydrogen-bond control of structure and conductivity of Langmuir films. *Physical. Review* E, Vol. 57, №6, (June 1998), p.p. 6835 – 6839, ISSN 1063-651X

[33] Luppi, M. & Ossicini S. (2005). Ab initio study on oxidized silicon clusters and silicon nanocrystals embedded in SiO_2: Beyond the quantum confinement effect. Phys. Rev. B V.71, (January 2005), p.p. 035340(1-15), ISSN 1098-0121

[34] Ma, Zhixun; Liao, Xianbo; Kong, Guanglin & Chu, Junhao (2000) Raman scattering of nanocrystalline silicon embedded in SiO_2. *Science in China* A, Vol.43, (2000), p.p. 414-420

[35] Min, R .B. & Wagner, S. (2002), Nanocrystalline silicon thin-film transistors with 50-nm-thick deposited channel layer, 10 $cm^2 V^{-1}s^{-1}$ electron mobility and 10^8 on/off current ratio *Applied Physics A Materials Science &Processing*, Vol. 74, (August 2001), p.p.541–543 (DOI) 10.1007/s003390100927

[36] Moliton, A. (2007) *Applied Electromagnetism and Materials*, Ch.1, p.8. Springer Science and Business Media. ISBN-10: 0-387-38062-0

[37] Nakajima, T. (1971) *Annual Report, Conference on Electric Insulation and Dielectric Phenomena* (Washington, D.C., National Academy of Sciences, 1972), p. 168.

[38] Namikawa. H. (1975).Characterization of the diffusion process in oxide glasses based on the correlation between electric conduction and dielectric relaxation. Journal of Non-Crystalline Solids, Vol.18, №2, (September 1975), p.p.173-195, ISSN 0022-3093.

[39] Nogami, M. & Abe, Y. (1997). Evidence of water-cooperative proton conduction in silica glasses. *Physical Review* B, Vol. 55, №18, (May 1997), p.p.12108 - 12112, ISSN 0163-1829

[40] Nogami, M.; Nagao, R. & Wong, C. (1998). Proton Conduction in Porous Silica Glasses with High Water Content. *Journal of Physical Chemistry* B, Vol. 102, (July 1998), p.p. 5772-5775, S1089-5647

[41] Pickering, C.; Beale, M. I. J.; Robbins, D. J.; Pearson, P. J. & Greef. R. (1984). Optical studies of the structure of porous silicon films formed in p-type degenerate and non- degenerate silicon. *Journal Physics* C: *Solid State Physics*, Vol.17, (August 1984) p.p.6535-6552, ISSN 0022-3719

[42] Puzder, A.; Williamson, A.J.; Grossman, J.C. & Galli G. (2002). Surface Chemistry of Silicon Nanoclusters. *Physical Review Letters*, Vol. 88, (2002), p.p.097401(1-4), ISSN 0031-9007

[43] Richter, H.; Wang, Z. & Ley L. (1981). The one phonon Raman spectrum in microcrystalline silicon. *Solid State Communications*, Vol.39, №5, (May 1981), p.p.625-629, ISSN 0038-1098

[44] Saadane, O.; Lebib, S.; Kharchenko, A.V.; Longeaud, C. & R. Roca I Cabarrocas. (2003) Structural, opical and electronic properties of hydrogenated polymorphous silicon films deposited from silane-hydrogen and silane-helium mixtures. *Journal of Applied Physics*, Vol. 93, №11, (June 2003), p.p.9371 – 9379, ISSN 0021-8979

[45] Schrøder, T. B. & Dyre. J. C. (2002). Computer simulations of the random barrier model. *Physical Chemistry and Chemical Physics*, Vol.4, (June 2002), p.p. 3173–3178

[46] Schrøder, T. B. & Dyre J. C.(2008). AC Hopping Conduction at Extreme Disorder Takes Place on the Percolating Cluster *Physical Review Letters,* Vol.101, (July 2008) p.p.025901(1-4), ISSN 0031-9007

[47] Schuppler, S.; Friedman, S.L.; Marcus, M.A.; Adler, D.L.; Xie, Y. H.; Ross, F.M.; Chabal, Y.J.; Harris, T.D.; Brus, L.E.; Brown, W.L.; Chaban, E.E.; Szajowski, P.E.; Christman, S.B. & Citrin, P.H. (1995). Size, shape and composition of luminescent species in oxidized Si nanocrystals and H-passivated porous Si. *Physical Review* B, Vol.52, p.p. 4910-4925, ISSN 1098-0121

[48] Stuart B. (2004). *Infrared Spectroscopy: Fundamentals and Applications*, John Wiley & Sons, Ltd., ISBN 0-470-85427-8

[49] Eds. by Tompkins, G. H. & Irene, E.A. (2005). *Handbook of ellipsometry*. p.p. 282-289. William Andrew publishing, Springer-Verlag GmbH & Co. KG. New York, Heidelberg. ISBN: 0-8155-1499-9 (William Andrew, Inc.), ISBN: 3-540-22293-6 (Springer-Verlag GmbH & Co. KG)

[50] De la Torre, J.; Bremond, G.; Lemiti, M.; Guillot , G.; Mur, P. & Buffet. N. (2006) Silicon nanostructured layers for improvement of silicon solar cells efficiency: A promising perspective. Materials Science and Engineering C Vol. 26, (January 2006), p.p. 427–430, ISSN 0928-4931

[51] Tsang, J.C.; Tischler, M.A. & Collins R.T. (1992). Raman scattering from H and O terminated porous Si. *Applied Physics Letters*, Vol.60, №18, (May 1992) p.p. 2279-2281, ISSN 0003-6951

[52] Tsu, R.; Shen, H. & Dutta M. (1992). Correlation of Raman and photoluminescence spectra of porous silicon. *Applied Physics Letters,* Vol.60, №1, (January1992), p.p. 112-114, ISSN 0003-6951

[53] Tsu, R.; Babić, D. & Ioriatti, L. Jr. (1997). Simple model for the dielectric constant of nanoscale silicon particle. *Journal Applied Physics,* Vol. 82, № 3, (August 1997), p.p.1327 – 1329, ISSN 0021-8979

[54] Tsu, R. (2000) Phenomena in silicon nanostructure devices. *Applied Physics* A Vol.71, (September 2000) p.p.391–402, DOI 10.1007/s003390000552

[55] Urbach, B.; Axelrod, E. & Sa'ar A. (2007). Correlation between transport, dielectric, and optical properties of oxidized and nonoxidized porous silicon *Physical Review* B, Vol. 75, №20, (May 2007) , p.p. 205330(11) , ISSN 1098-0121

[56] Voutsas, A.T.; Hatalis, M.K.; Boyce, J. & Chiang A. (1995). Raman spectroscopy of amorphous and microcrystalline silicon films deposited by low-pressure chemical

vapor deposition *Journal of Applied Physics,* Vol.78, №12, (December 1995), p.p. 6999-7005, ISSN 0021-8979

[57] Wang, K.; Chen, H. & Shen, W.Z. (2003). AC electrical properties of nanocrystalline silicon thin films. *Physica* B, Vol. 336, (April 2003), p.p. 369-378, ISSN 0921-4526

[58] Wang, W. & MacDiarmid, A. (2002), New synthesis of phenil/phenil end-capped tetraaniline in the leucoemeraldine oxidation states. *Synthetic metals,* Vol. (2002) 129, p.p. 199-205, ISSN

[59] Wovchko, E. A.; Camp, J. C.; Glass, J. A. Jr. & Yates, J. T. Jr. (1995). Active sites on SiO_2: role in CH_30H decomposition. Langmuir Vol.11, №7, (1995), p.p.2592-2599, ISSN 0743-7463

[60] G. Zuter.(1980) Dielectric and Optical Properties of SiO_x. *Physica Status Solidi* (a) Vol. 59, (April 1980), p.p. K109 –K113

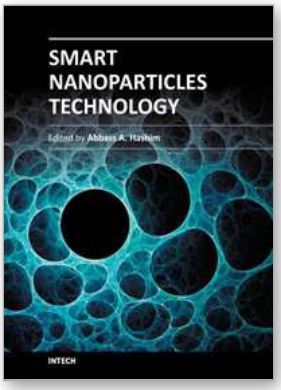

Smart Nanoparticles Technology

Edited by Dr. Abbass Hashim

ISBN 978-953-51-0500-8
Hard cover, 576 pages
Publisher InTech
Published online 18, April, 2012
Published in print edition April, 2012

In the last few years, Nanoparticles and their applications dramatically diverted science in the direction of brand new philosophy. The properties of many conventional materials changed when formed from nanoparticles. Nanoparticles have a greater surface area per weight than larger particles which causes them to be more reactive and effective than other molecules. In this book, we (InTech publisher, editor and authors) have invested a lot of effort to include 25 most advanced technology chapters. The book is organised into three well-heeled parts. We would like to invite all Nanotechnology scientists to read and share the knowledge and contents of this book.

How to reference

In order to correctly reference this scholarly work, feel free to copy and paste the following:

Nickolay N. Kononov and Sergey G. Dorofeev (2012). Dielectric and Transport Properties of Thin Films Deposited from Sols with Silicon Nanoparticles, Smart Nanoparticles Technology, Dr. Abbass Hashim (Ed.), ISBN: 978-953-51-0500-8, InTech, Available from: http://www.intechopen.com/books/smart-nanoparticles-technology/dielectric-and-transport-properties-of-thin-films-deposited-on-solid-substrates-from-sols-with-silic

INTECH
open science | open minds

InTech Europe
University Campus STeP Ri
Slavka Krautzeka 83/A
51000 Rijeka, Croatia
Phone: +385 (51) 770 447
Fax: +385 (51) 686 166
www.intechopen.com

InTech China
Unit 405, Office Block, Hotel Equatorial Shanghai
No.65, Yan An Road (West), Shanghai, 200040, China
中国上海市延安西路65号上海国际贵都大饭店办公楼405单元
Phone: +86-21-62489820
Fax: +86-21-62489821